Instant Tomography of Active Regions

Markus J. Aschwanden
Jean-Pierre Wuelser, Nariaki Nitta, & James Lemen
(LMSAL)

STEREO Science Working Group Meeting
Old Pasadena, CA, February 3-5, 2009
http://www.lmsal.com/~aschwand/ppt/2009_SWG_Pasasena_Tomo.ppt

Content of talk :

1) Stereoscopic reconstruction of 3D geometry of coronal loops

2) Electron density and temperature measurements

3) Instant stereoscopic tomography of active regions (ISTAR)

Relevant Publications:

-Aschwanden, Wuelser, Nitta, & Lemen 2008: “First 3D Reconstructions of Coronal Loops with the STEREO A+B Spacecraft:

I. Geometry (□2008, ApJ 679, 827)

II. Electron Density and Temperature Measurements (2008, ApJ 680, 1477)

III. Instant Stereoscopic Tomography of Active regions (2008, ApJ 694, Apr 1 issue)

May 2007

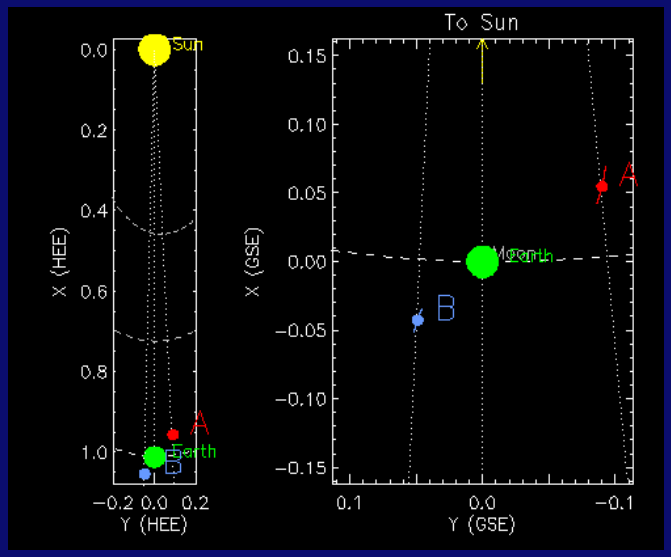

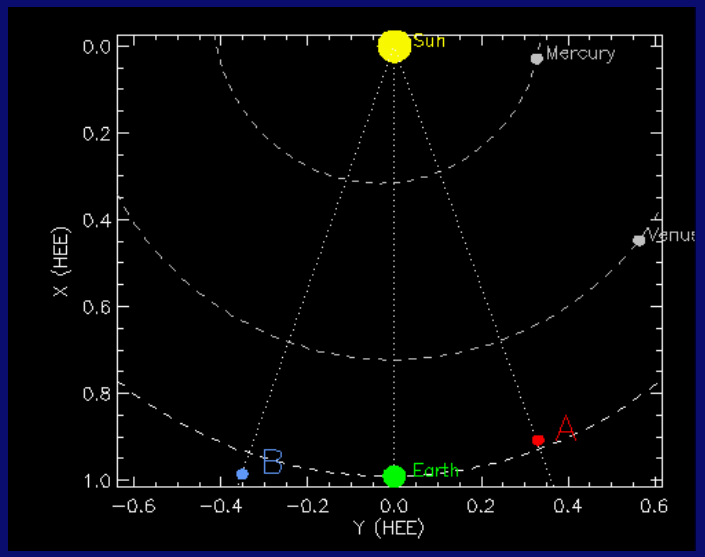

Nov 2007

STEREO A-B separation angles

(2007 is prime phase for small-angle stereoscopy)

Date	B (deg East)	A(deg West)	A-B(deg separation)
2007-Jan-1	0.151	0.157	0.009
2007-Feb-1	0.167	0.474	0.623
2007-Mar-1	0.169	1.061	1.229
2007-Apr-1	0.740	2.307	3.032
2007-May-1	1.888	4.213	6.089
2007-Jun-1	3.762	6.843	10.600
2007-Jul-1	6.196	9.810	16.004
2007-Aug-1	9.211	12.975	22.186
2007-Sep-1	12.525	15.871	28.396
2007-Oct-1	15.764	18.127	33.891
2007-Nov-1	18.830	19.744	38.574
2007-Dec-1	21.216	20.660	41.876
2008-Jan-1	22.837	21.182	44.018

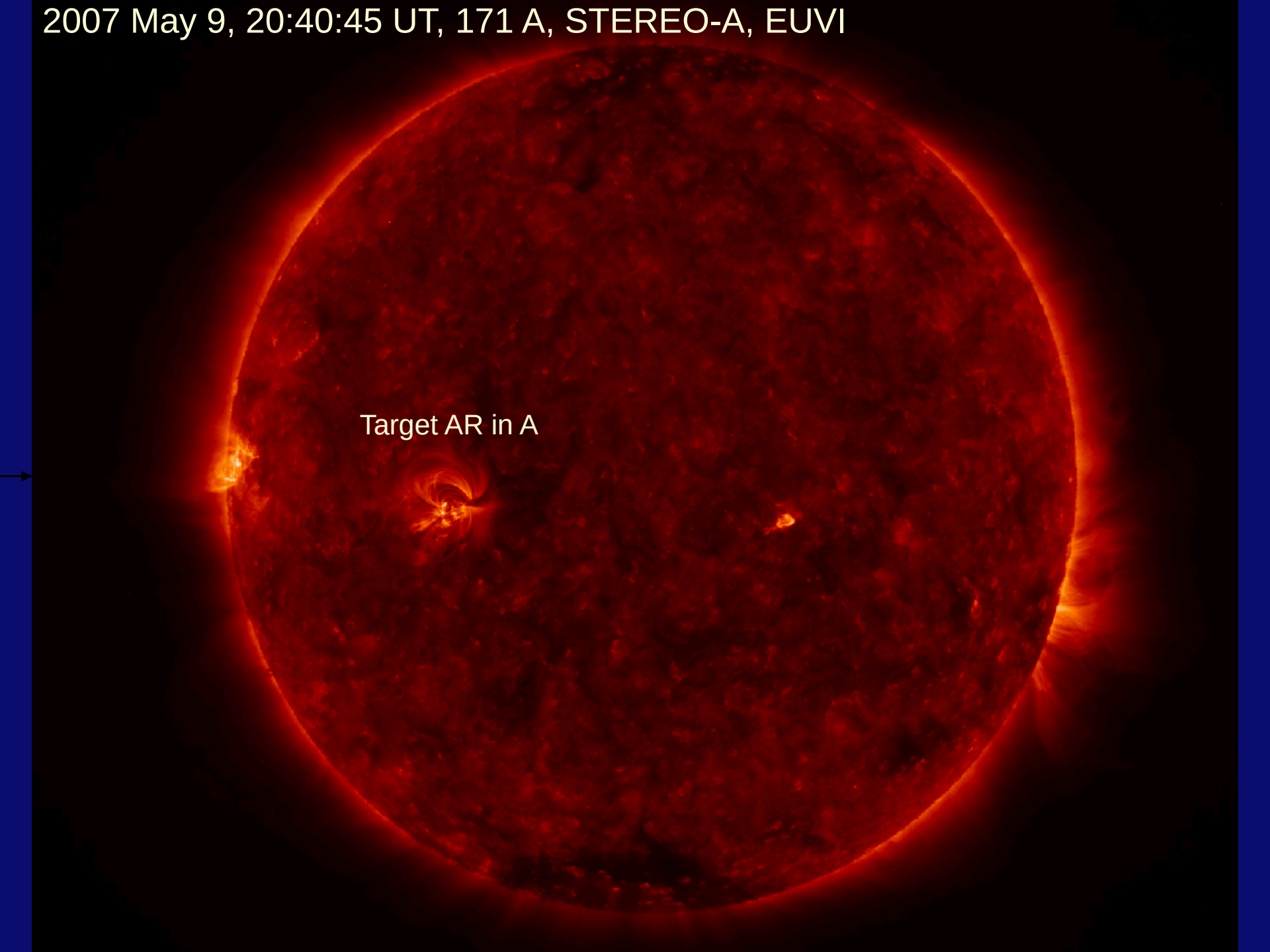
2007 May 9, 20:40:45 UT, 171 A, STEREO-A, EUVI
Target AR in A

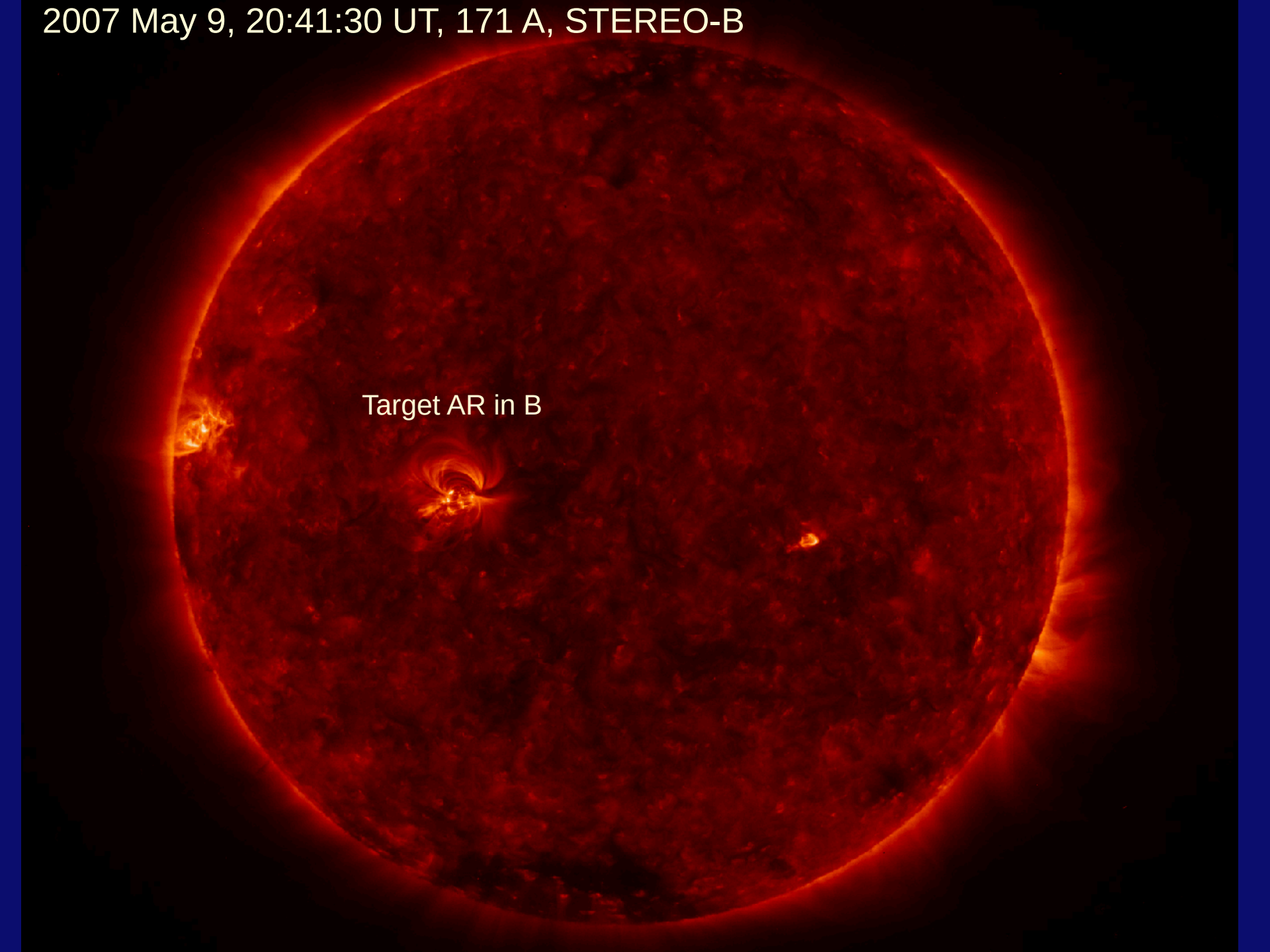
2007 May 9, 20:41:30 UT, 171 A, STEREO-B
Target AR in B

Coaligned STEREO image pair A+B with FOV of AR

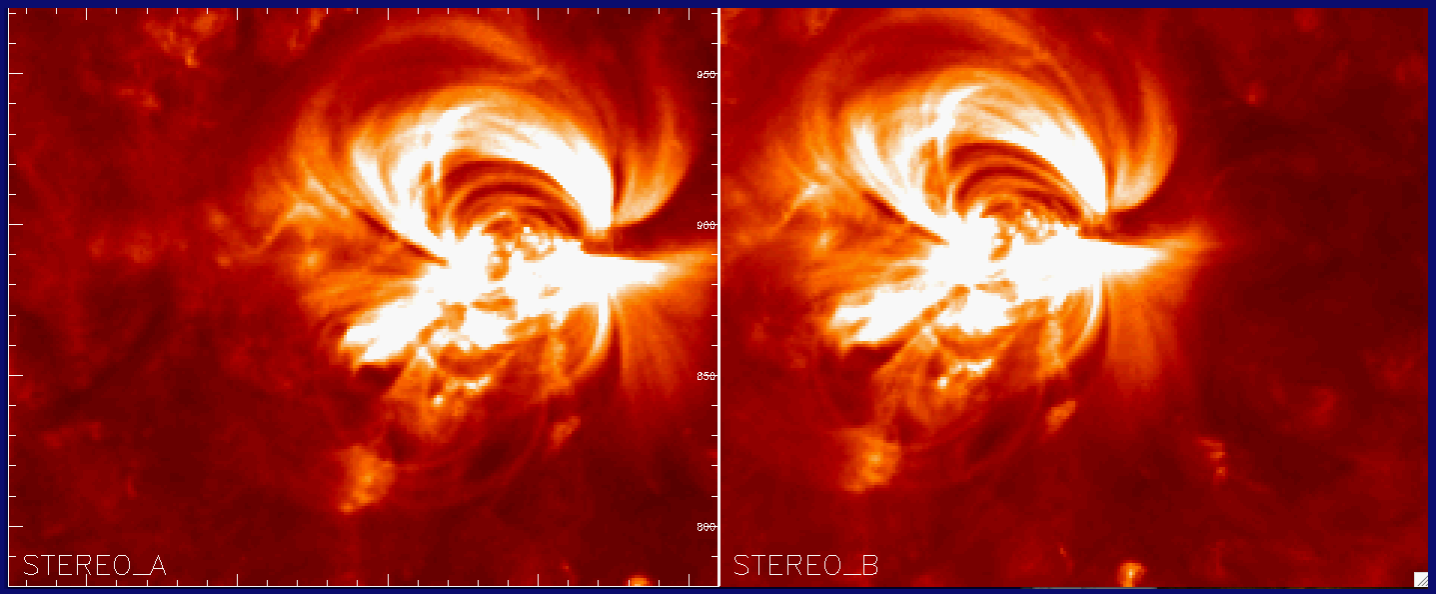

Highpass-filtered STEREO image pair A+B

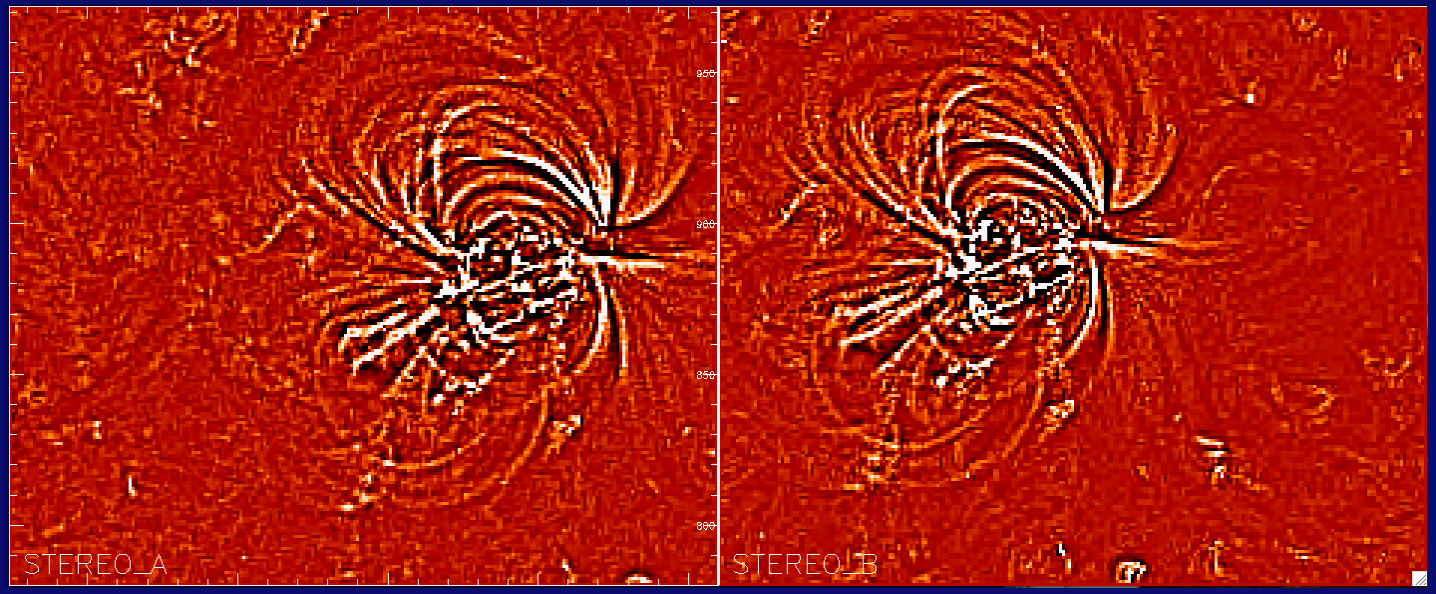

Image Highpass-Filtering and Loop Definition

Best S/N ratio, but widest loops

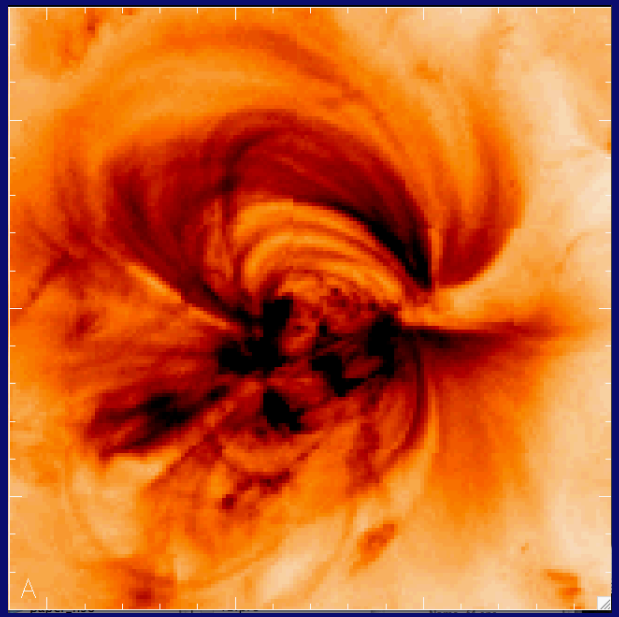

Unfiltered image (100% flux)

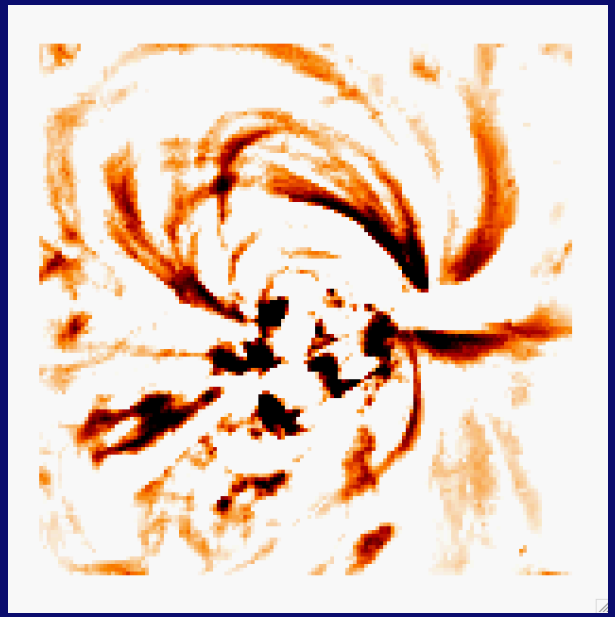

Higphass filter (w<21 pixel)

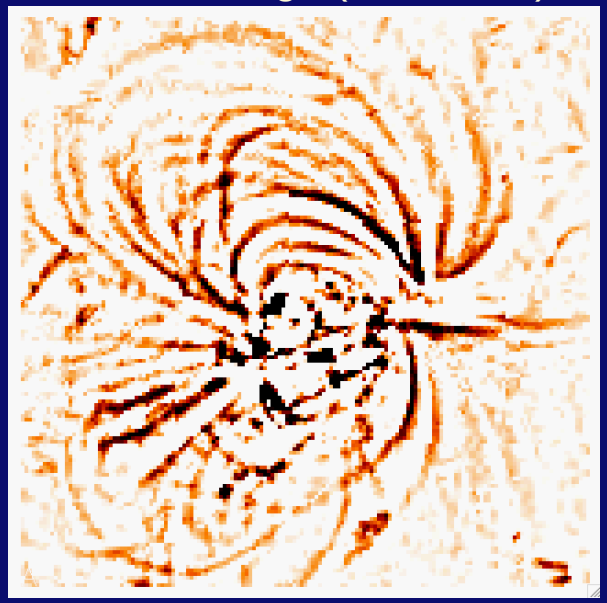

Highpass filter (w<7 pixel)

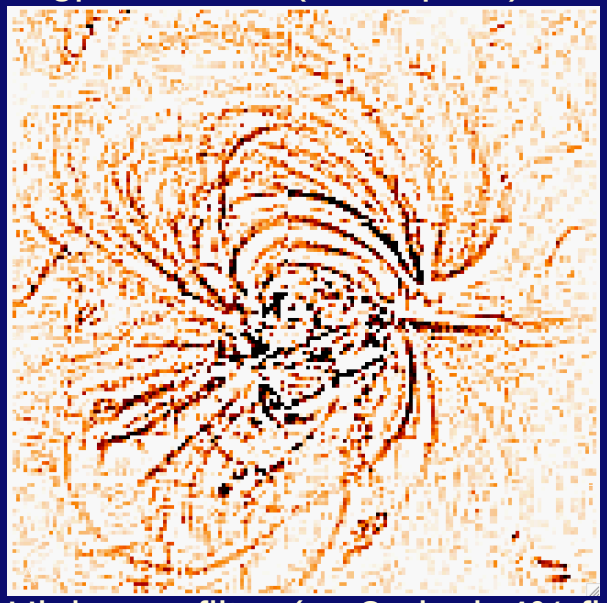

Highpass filter (w<3 pixel; 4% flux)

Lowest S/N ratio, but narrowest loops

Image Preprocessing: (1) Multi-scale filtering

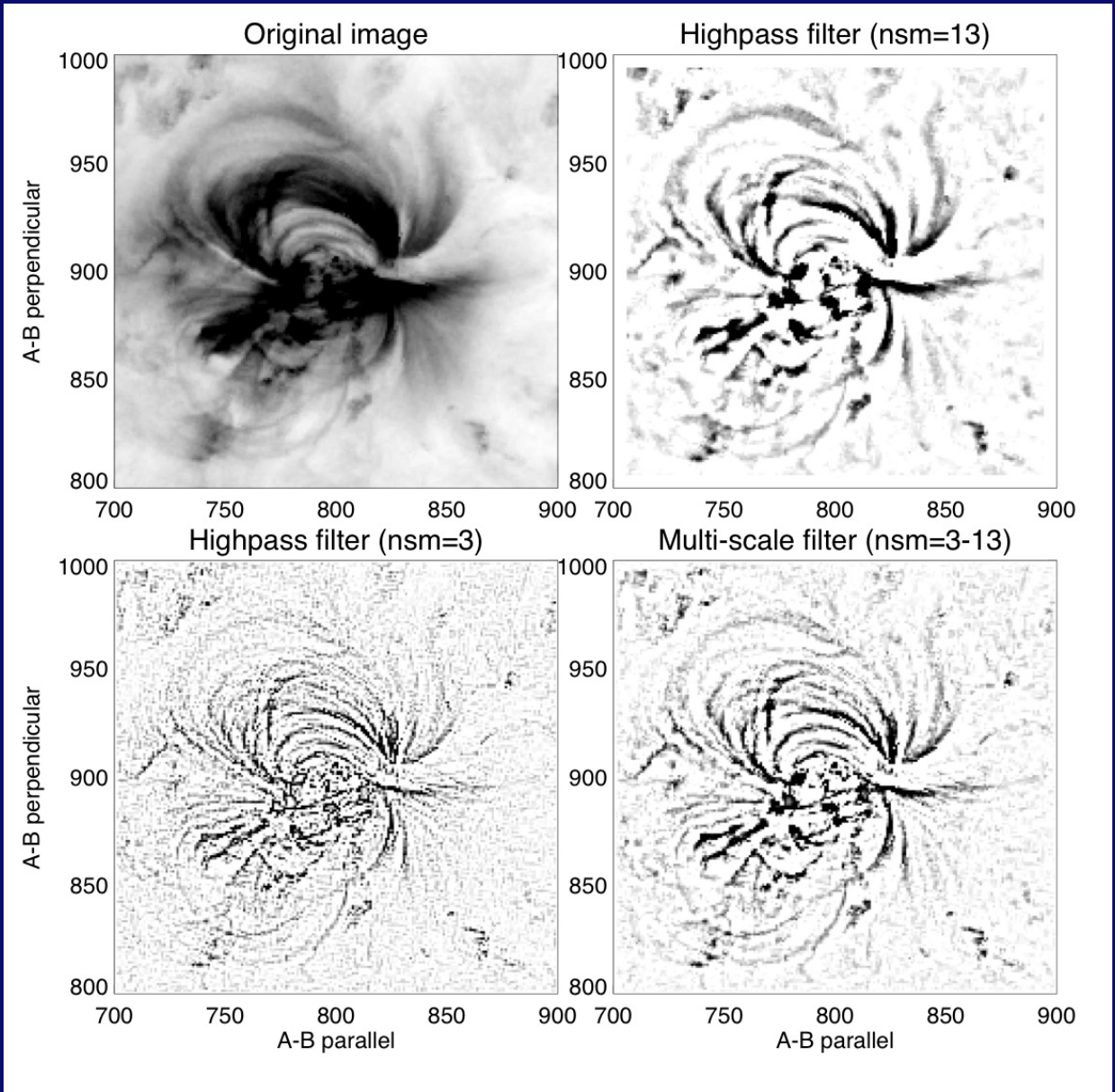

Image Preprocessing: (2) Image stacking

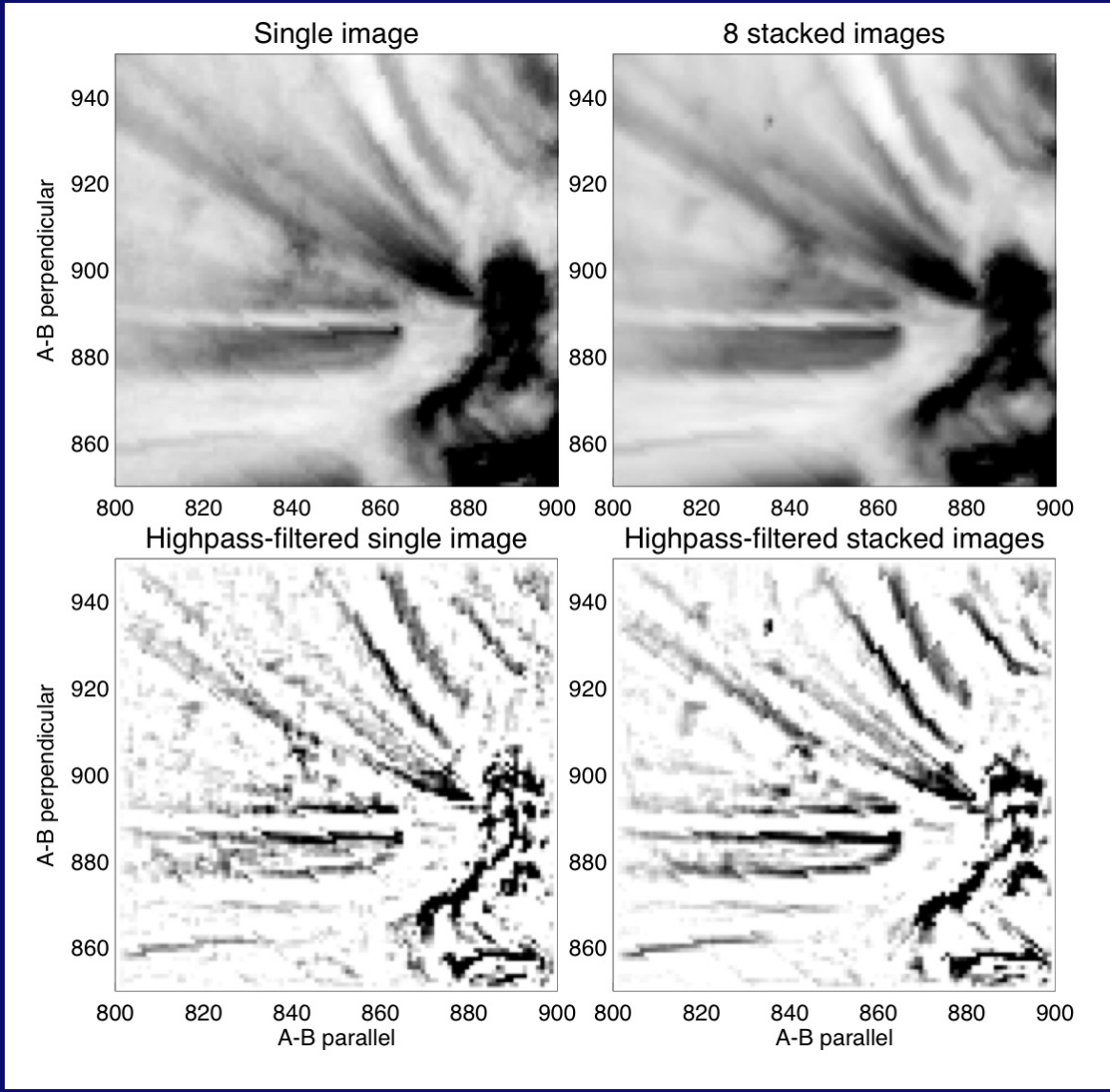

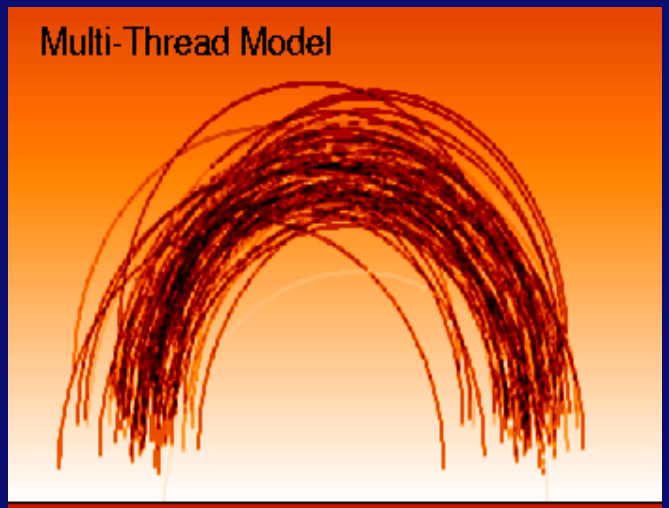

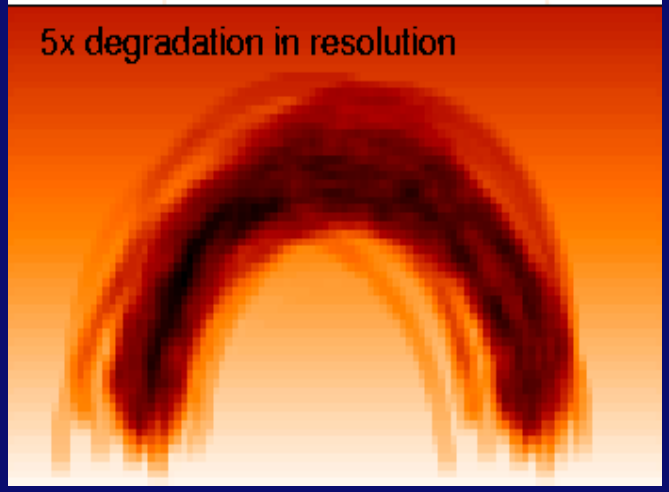

Concept of elementary loop strands and composite loops:

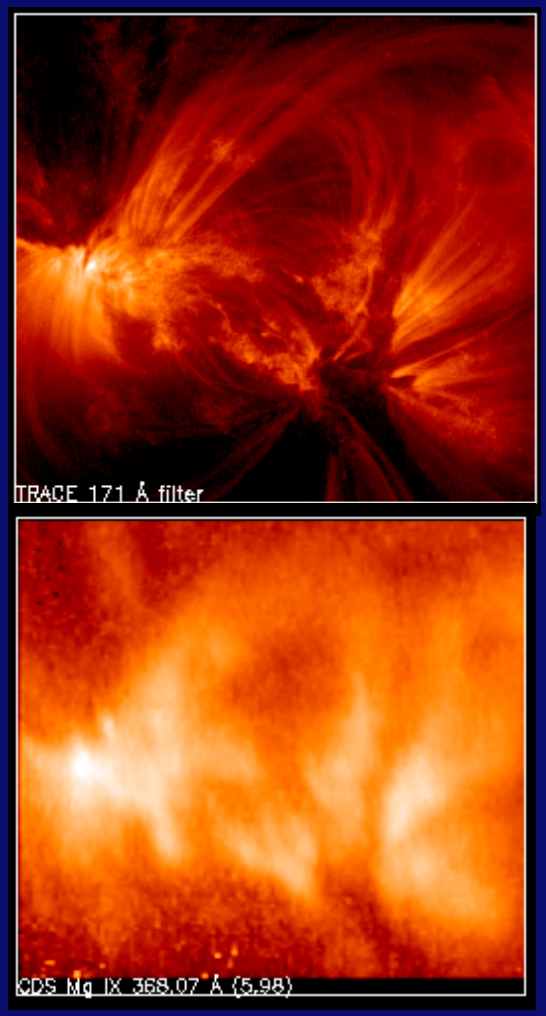

Simultaneous images recorded in EUV in near-identical temperature filters (e.g., TRACE 171 A vs CDS Mg IX, ~ 1.0 MK) reveal that a loop system observed with CDS (with a spatial resolution of ~4” pixel) is composed of at least 10 loop strands when imaged with TRACE (with a pixel size of 0.5” and spatial resolution of ~1”).

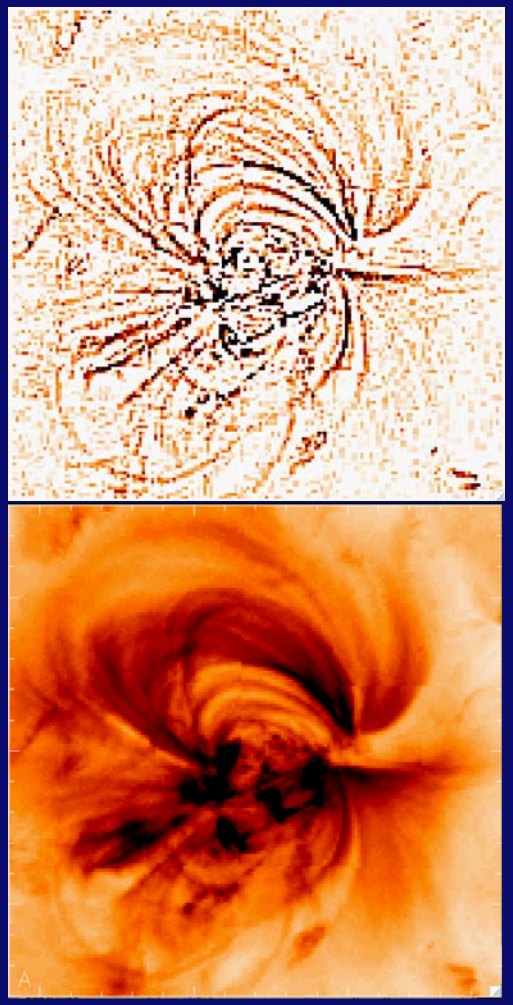

With a highpass filter we enhance the finest loop strands, but EUVI has a spatial resolution of 3.5” (2.2 EUVI pixels = 2500 km), and thus the finest structures seen with EUVI probably correspond to “composite” loops. TRACE found elementary (isothermal) loops for w<1500 km

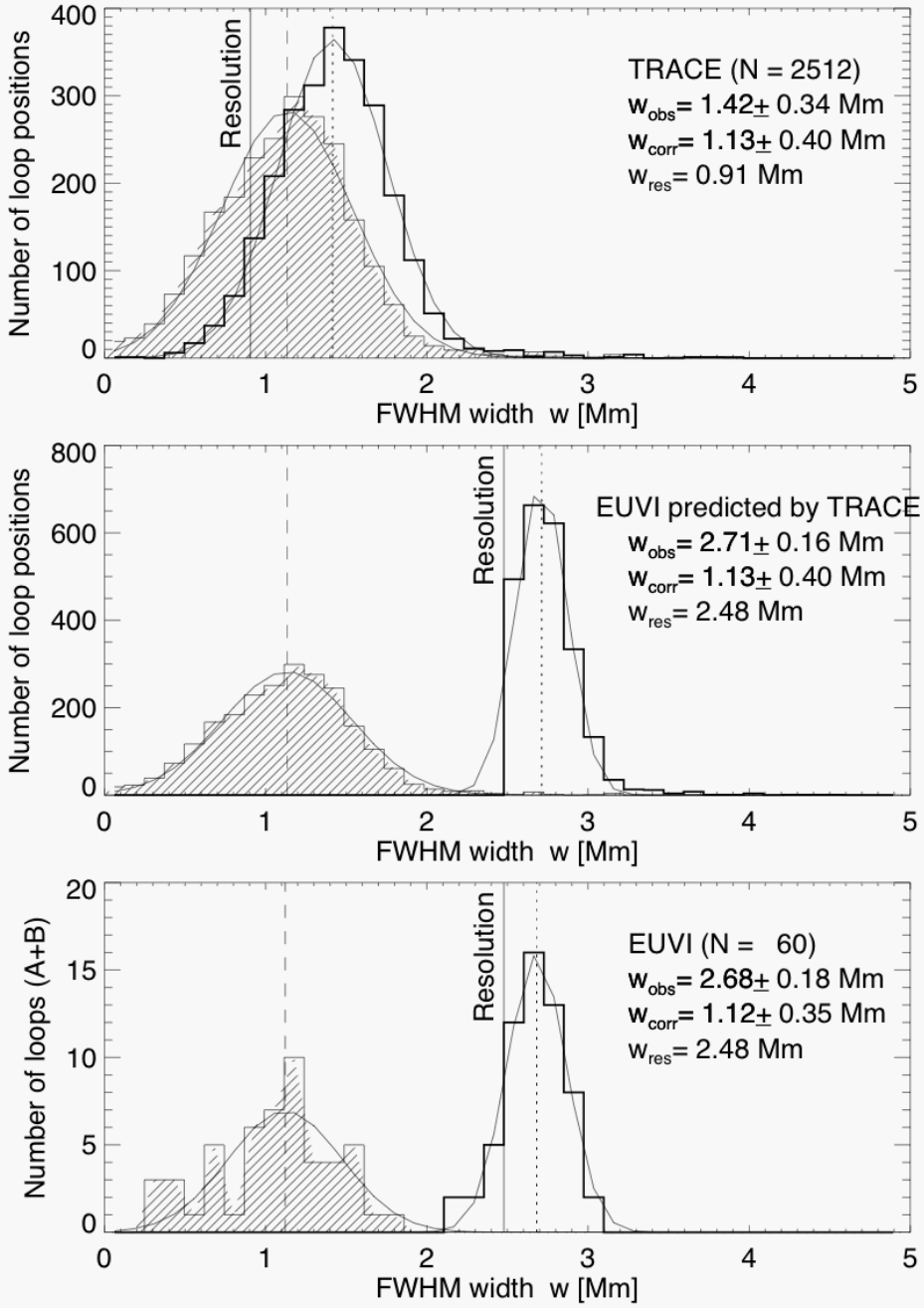

The fact that all analyzed loops in EUVI have a diameter close to the spatial resolution of EUVI indicates that they are unresolved and have smaller real diameters: d<2.5 Mm

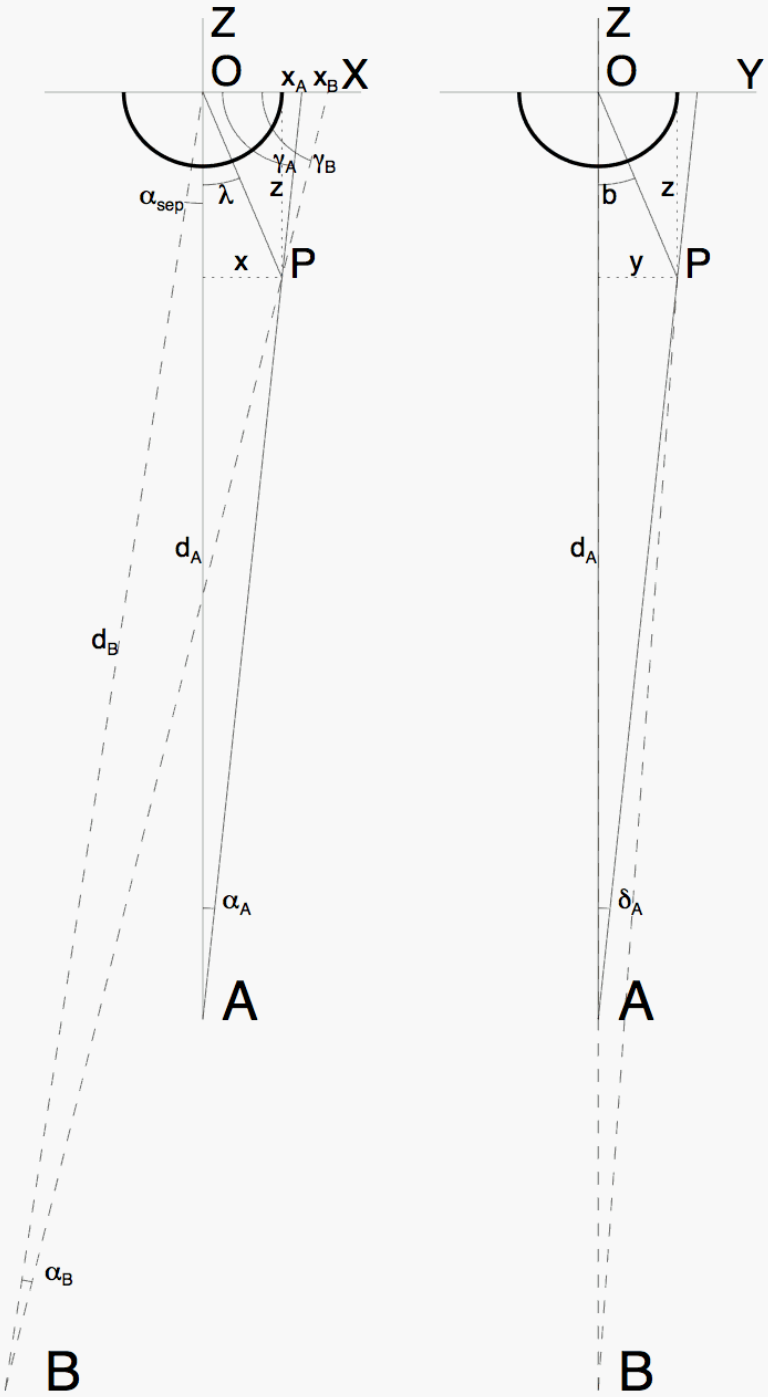

Observables:

d_A, d_B, α_A, α_B, δ_A, δ_B, α_{sep}

Trigonometric relations:

$$\gamma_A = \frac{\pi}{2} - \alpha_A$$

$$\gamma_B = \frac{\pi}{2} - \alpha_B - \alpha_{sep}$$

$$x_A = d_A \tan(\alpha_A)$$

$$x_B = d_B \frac{\sin(\alpha_B)}{\sin(\gamma_B)}$$

$$x = \frac{x_B \tan(\gamma_A) - x_A \tan(\gamma_B)}{\tan(\gamma_B) - \tan(\gamma_A)}$$

$$z = (x_A - x)\tan(\gamma_A)$$

$$y = (d_A - z)\tan(\delta_A)$$

$$r = \sqrt{x^2 + y^2 + z^2}$$

$$h = r - R_\circ$$

Calculated parameters:

x, y, z, r, h

Stereoscopic 3D Reconstruction

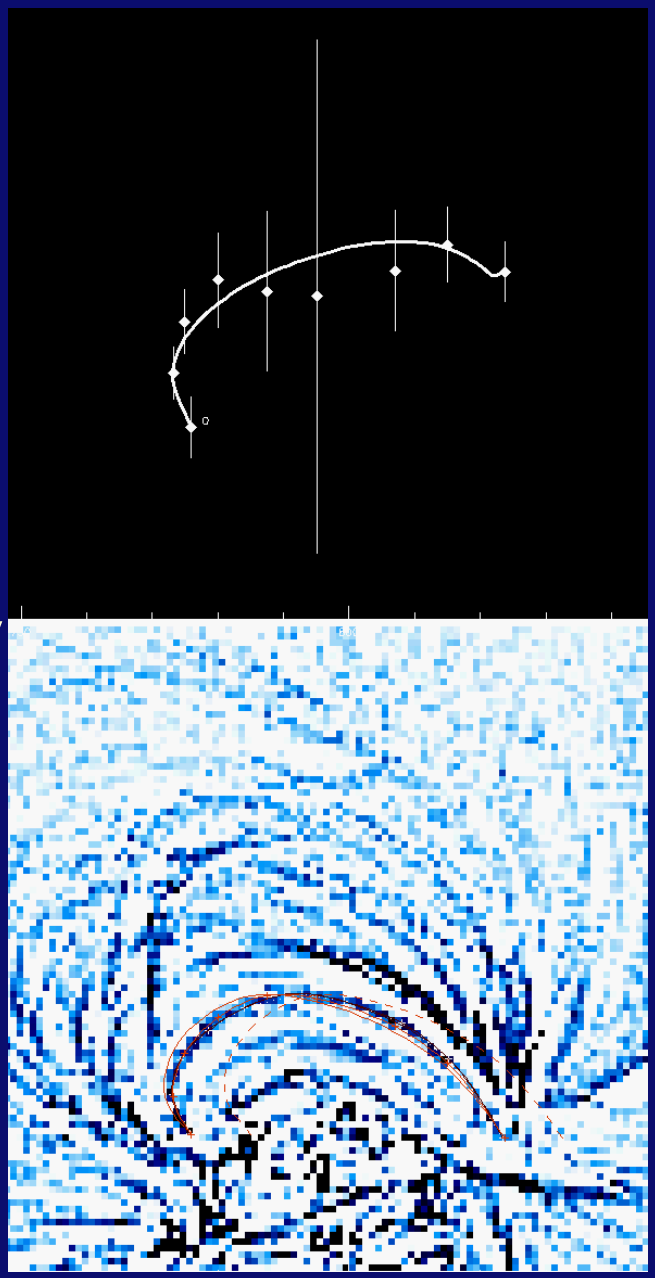

- Manual clicking on 4-8 loop positions in STEREO-A image (x_A,y_A)
- Manual clicking on 4-8 loop positions in STEREO-B image (x_B, y_B)
- Calculating (x,y,z) 3D coordinates from stereoscopic parallax
- Calculate stereoscopic error for each loop point $z \pm \sigma_z$
- Weighted polynomial fit z(s) (2nd-order) with s' the projected loop length coordinate s in [x,y] plane

Stereoscopic error in z-coordinate:

$$\sigma_z = \frac{1}{2}\sqrt{1+\tan(\vartheta[s_i])}$$

$$\tan(\vartheta[s_i]) = \frac{|\alpha_B(s_{i+1}) - \alpha_B(s_i)|}{|\delta_B(s_{i+1}) - \delta_B(s_i)|}$$

Error=1/2 pixel in NS direction
infinite in EW direction

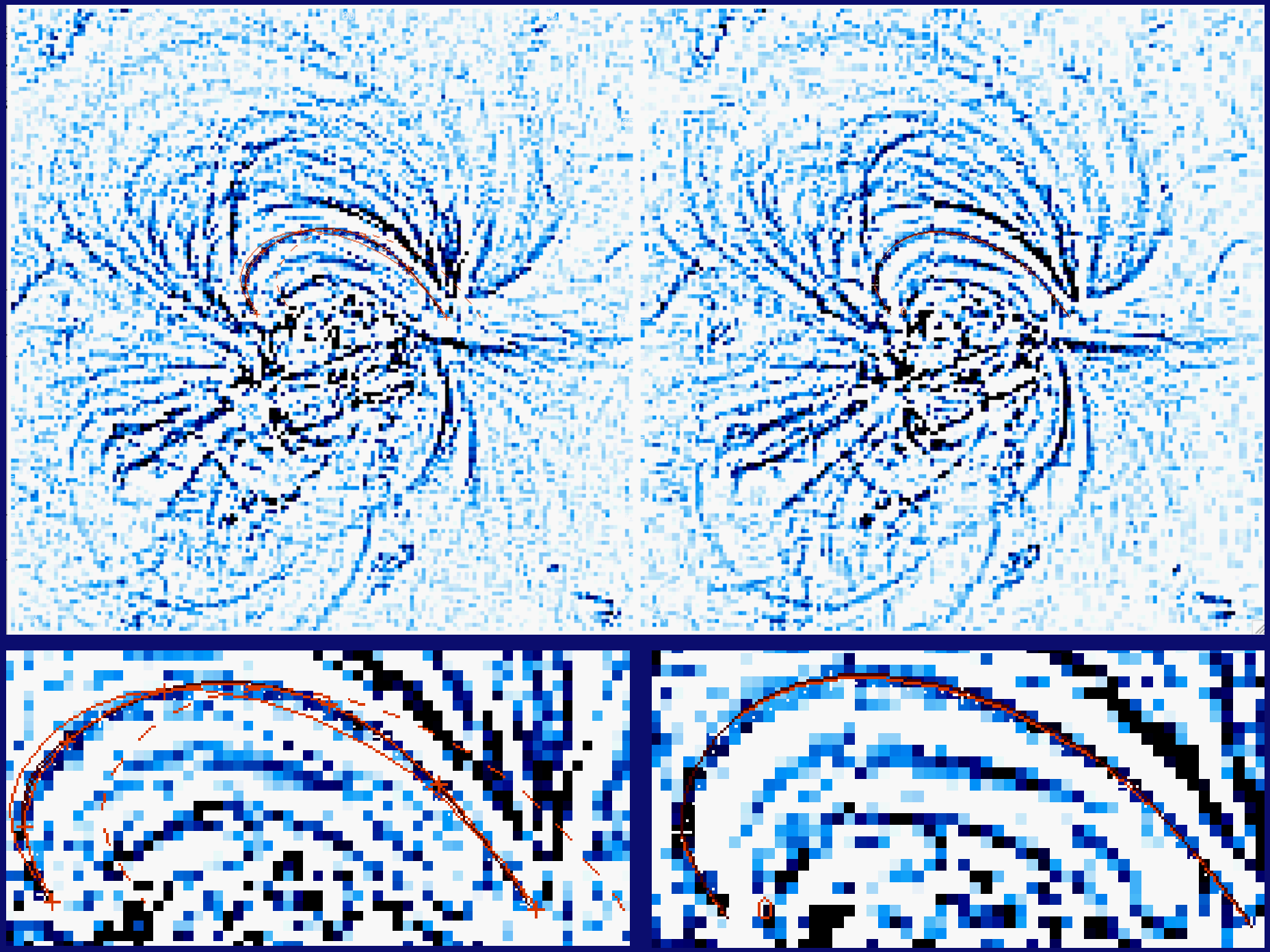

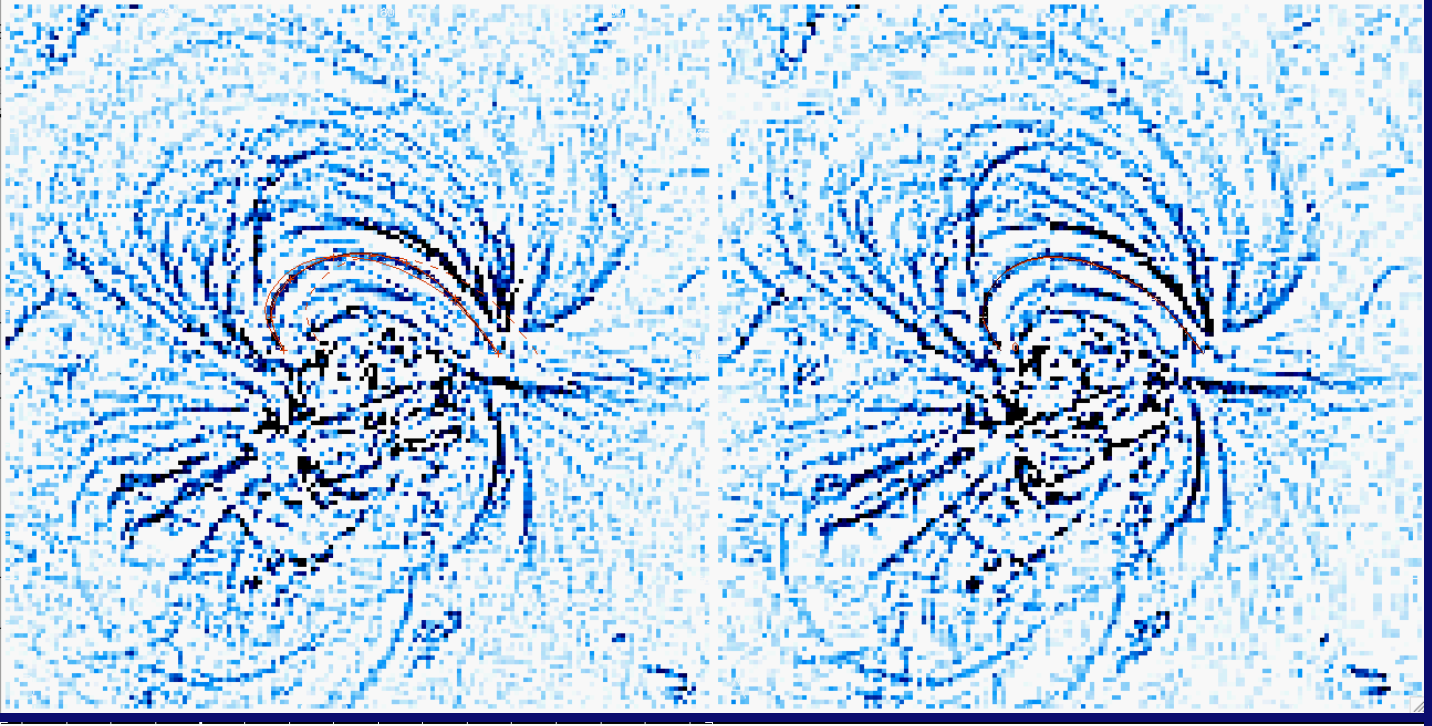

Highpass filter: subtract image smoothed with 3x3 boxcar

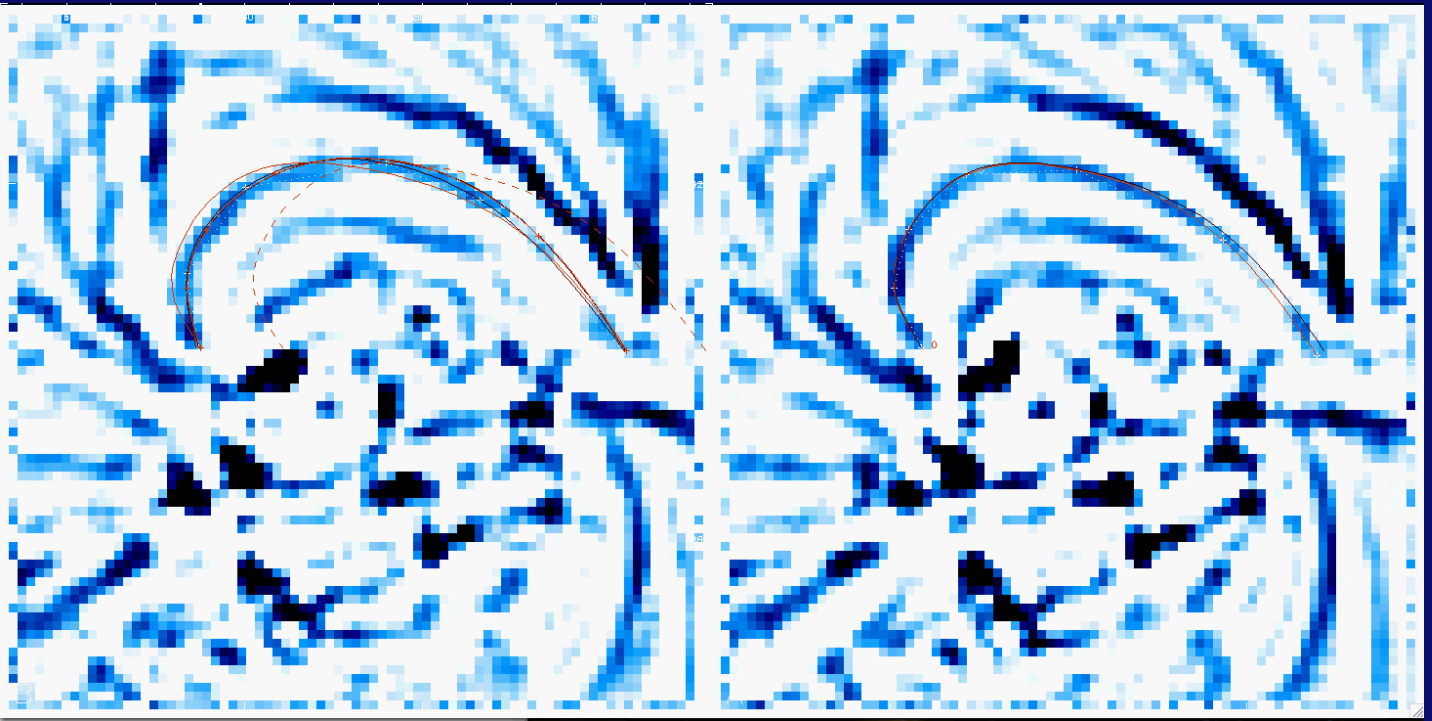

Highpass filter: subtract image smoothed with 5x5 boxcar

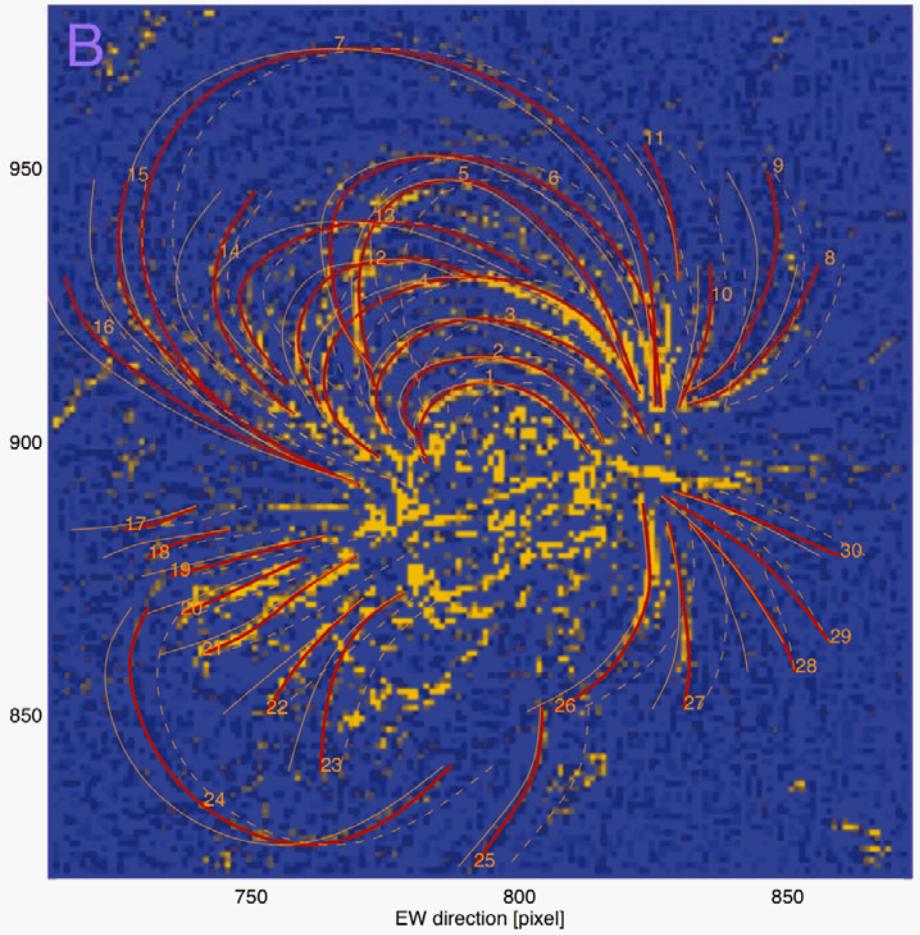
B
950
900
850
750
800
850
EW direction [pixel]

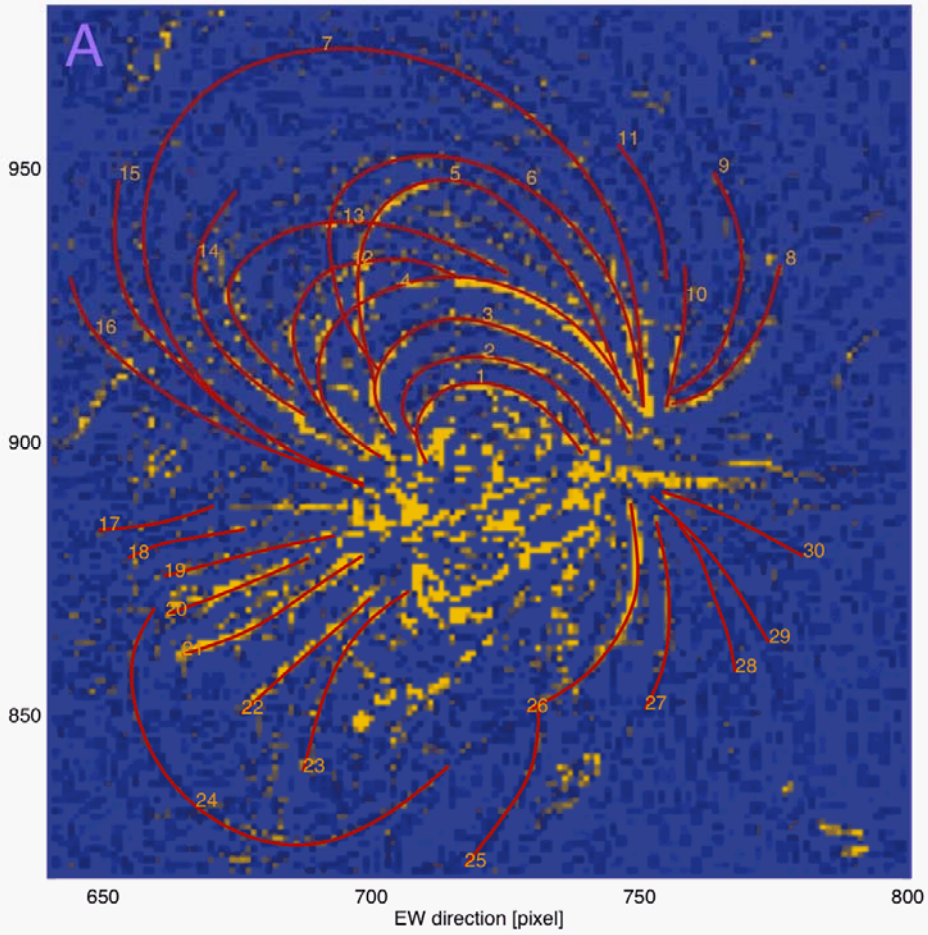
A
950
900
850
650
700
750
800
EW direction [pixel]

3D projections of loop geometries: [x,y] --> [x,z],[y,z]

Color: blue=short loops
red=midsize loops
yellow=long loops
white=longest loop

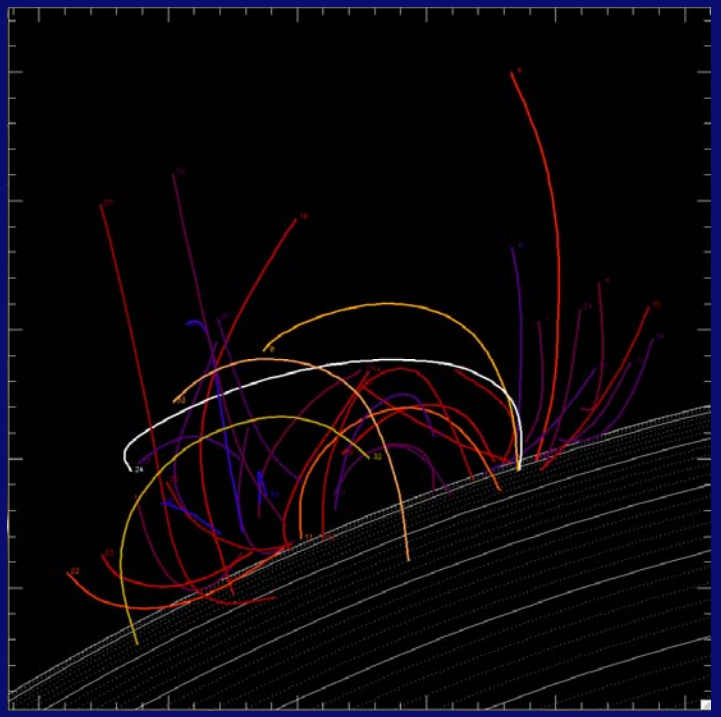

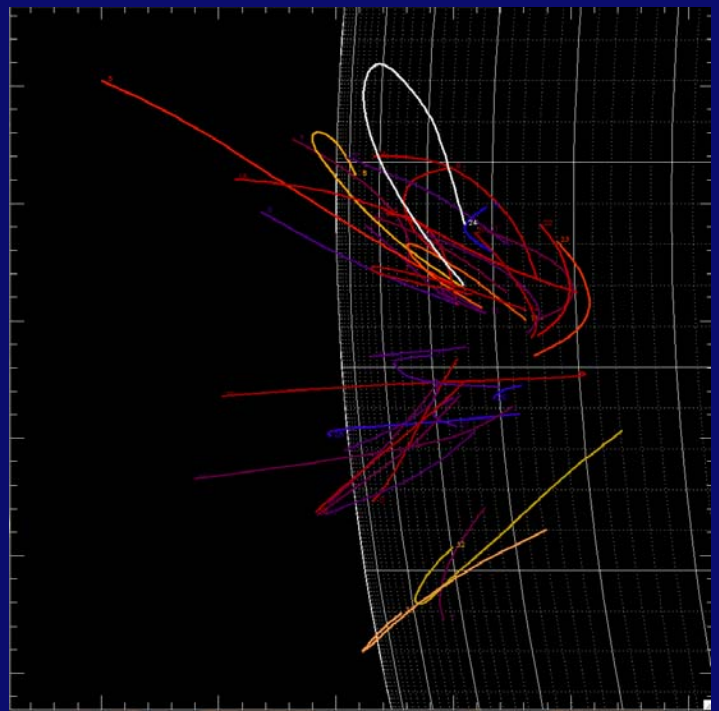

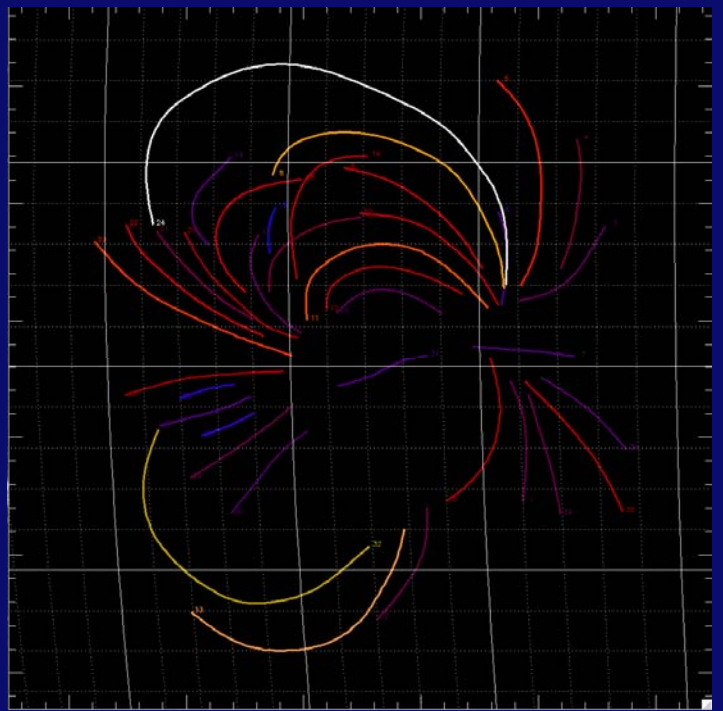

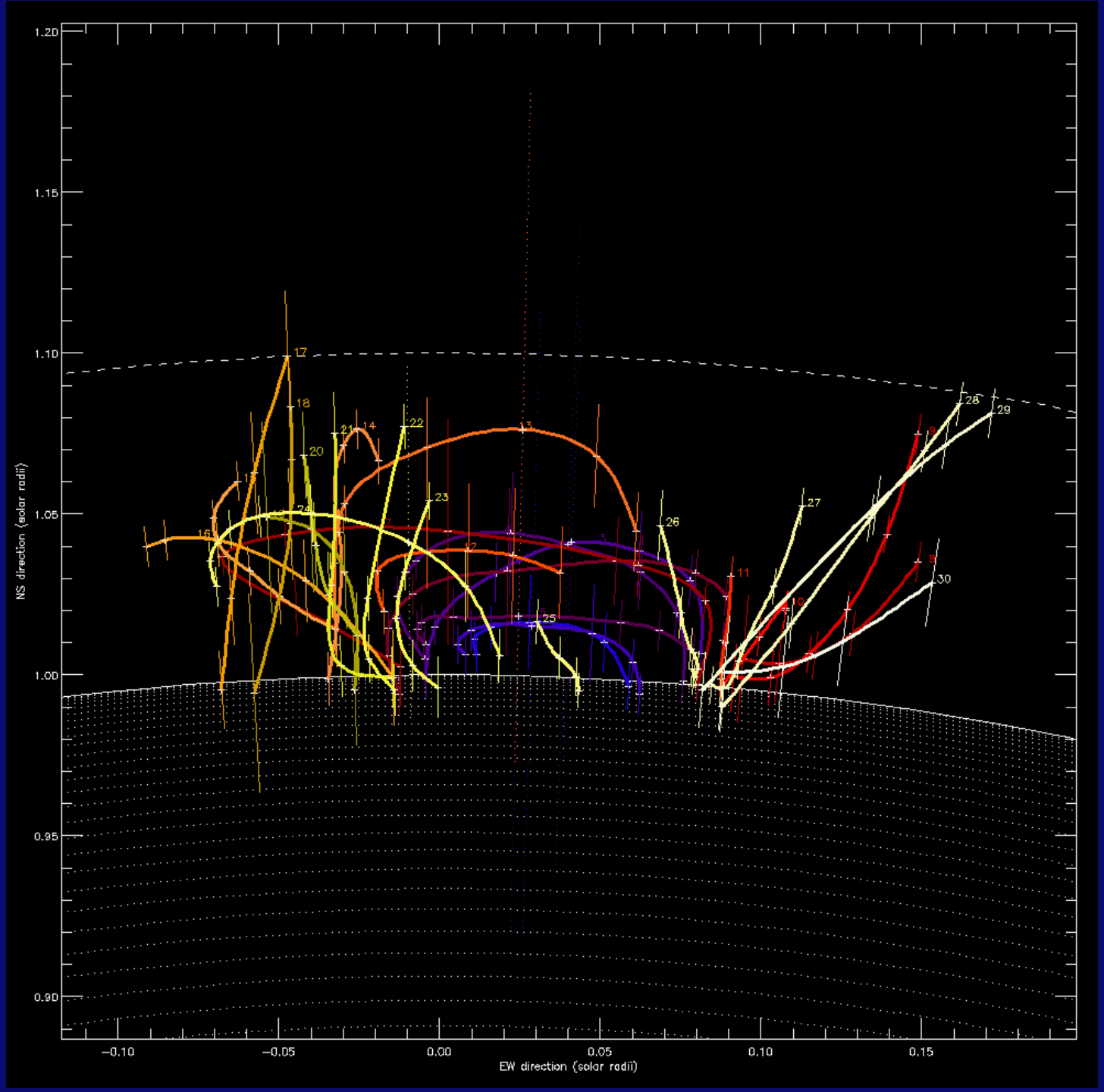

View in NS projection with errors of heights

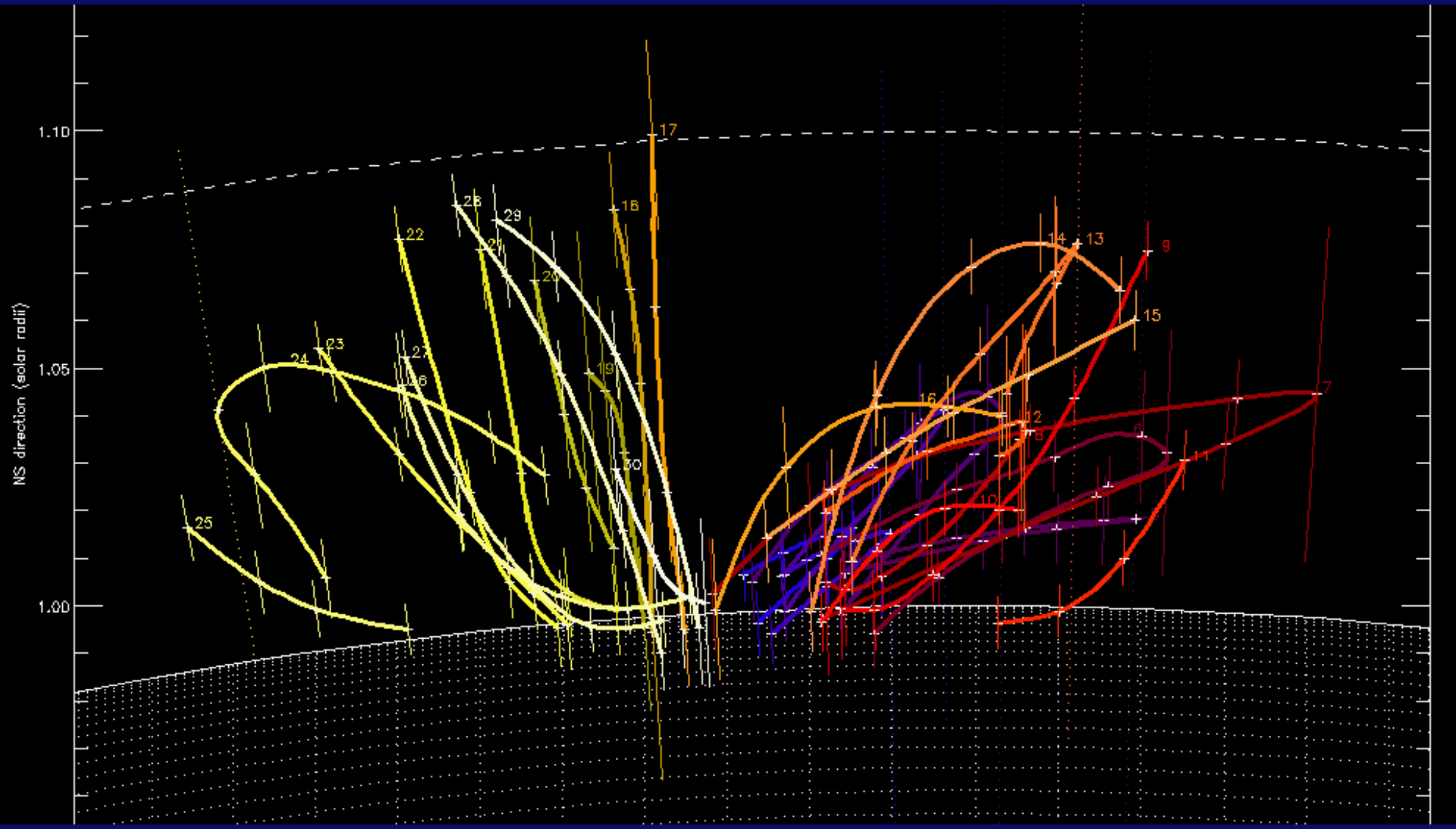

View in EW direction with stereoscopic height errors

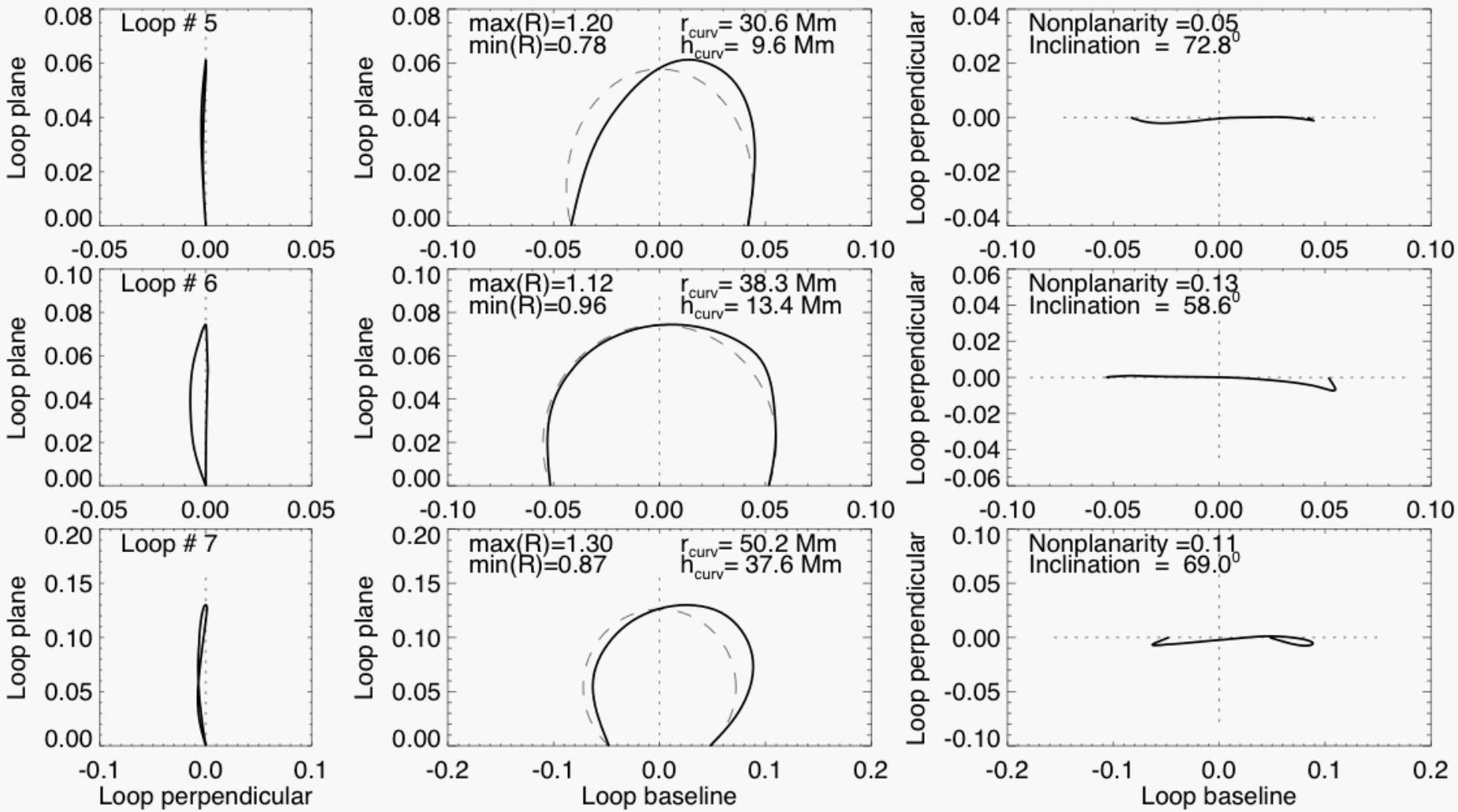

Circularity ratio: $C(s) = R(s)/r_{curv}$

Coplanarity ratio: $P(s)=y_{perp}(s)/r_{curv}$

Loop #	Maximum Height h_{max} [Mm]	Curvature radius r_{curv} [Mm]	Center offset h_{curv} [Mm]	Inclination angle ϑ [deg]	Circularity ratio C	Coplanarity ratio P
1	11.6	17.0	1.2	51.3	0.92−1.11	0.09
2	10.9	19.4	0.3	56.7	0.97−1.19	0.08
3	29.8	30.5	4.3	35.7	0.90−1.12	0.03
4	30.7	30.9	10.7	42.9	0.96−1.11	0.07
5	13.0	30.6	9.6	72.8	0.78−1.20	0.05
6	26.2	38.3	13.4	58.6	0.96−1.12	0.13
7	32.3	50.2	37.6	69.0	0.87−1.30	0.11

Hydrostatic Modeling

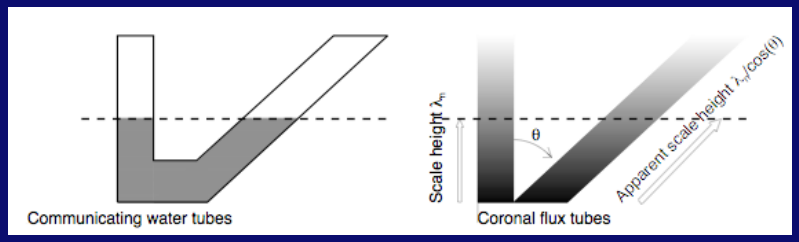

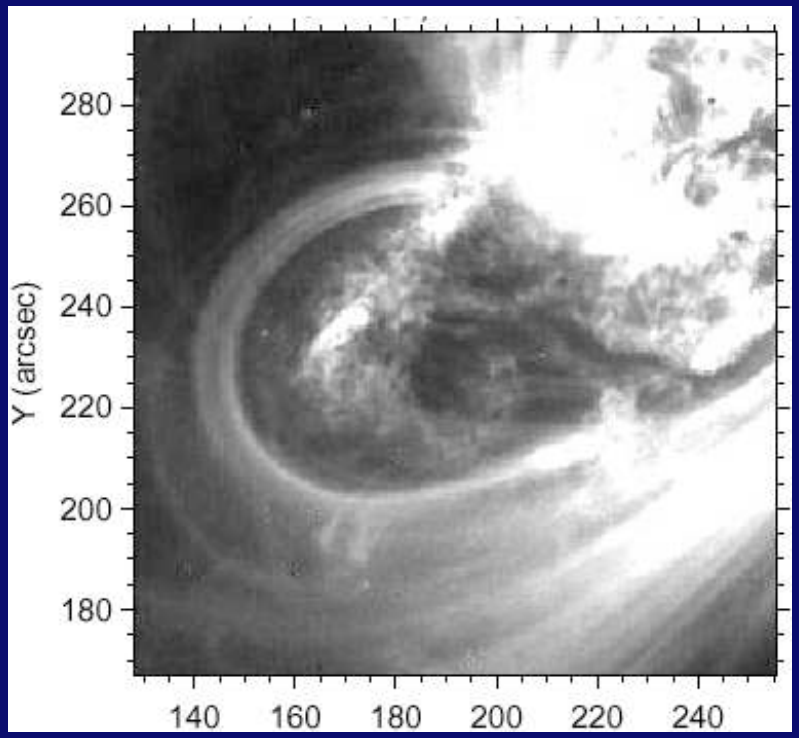

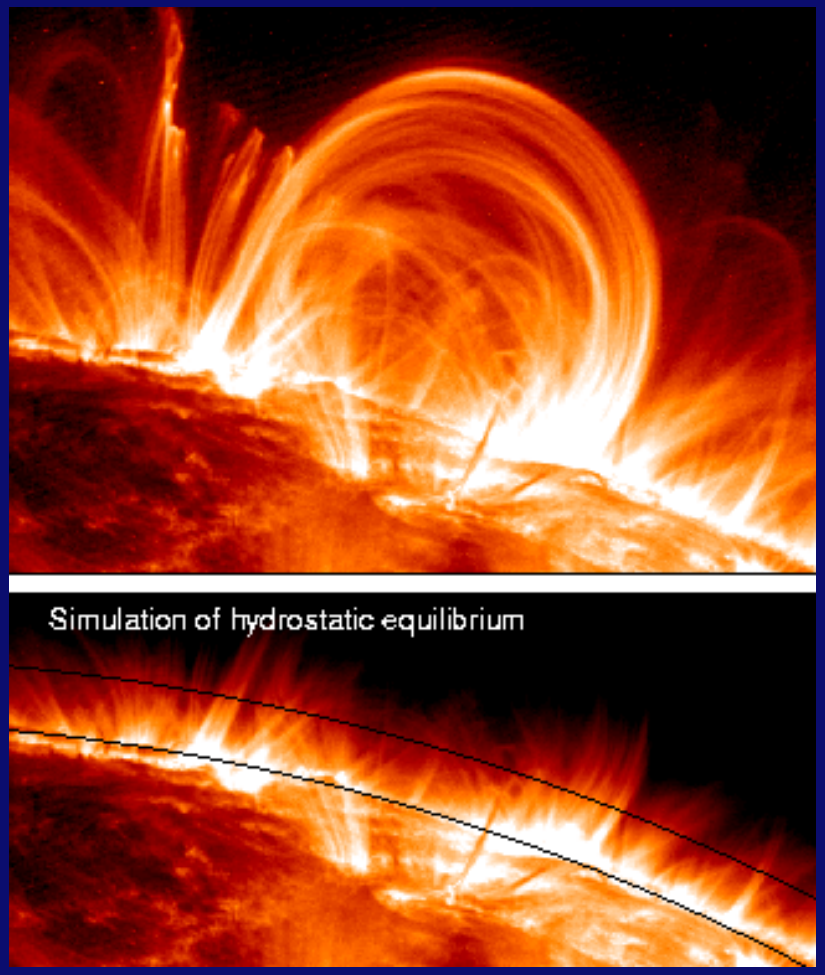

The true vertical scale height can only be determined from proper (stereoscopic) 3D reconstruction of the loop geometry:
--> Tests of hydrostatic equilibrium vs. super-hydrostatic dynamic states

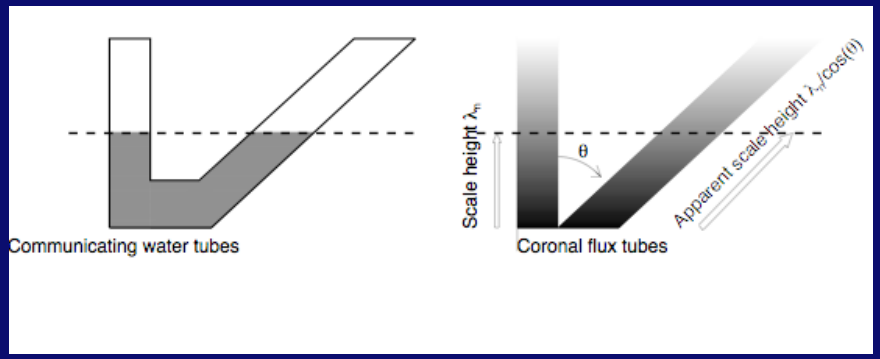

Loop #	Maximum Height h_{max} [Mm]	Curvature radius r_{curv} [Mm]	Center offset h_{curv} [Mm]	Inclination angle ϑ [deg]
1	11.6	17.0	1.2	51.3
2	10.9	19.4	0.3	56.7
3	29.8	30.5	4.3	35.7
4	30.7	30.9	10.7	42.9
5	13.0	30.6	9.6	72.8
6	26.2	38.3	13.4	58.6
7	32.3	50.2	37.6	69.0

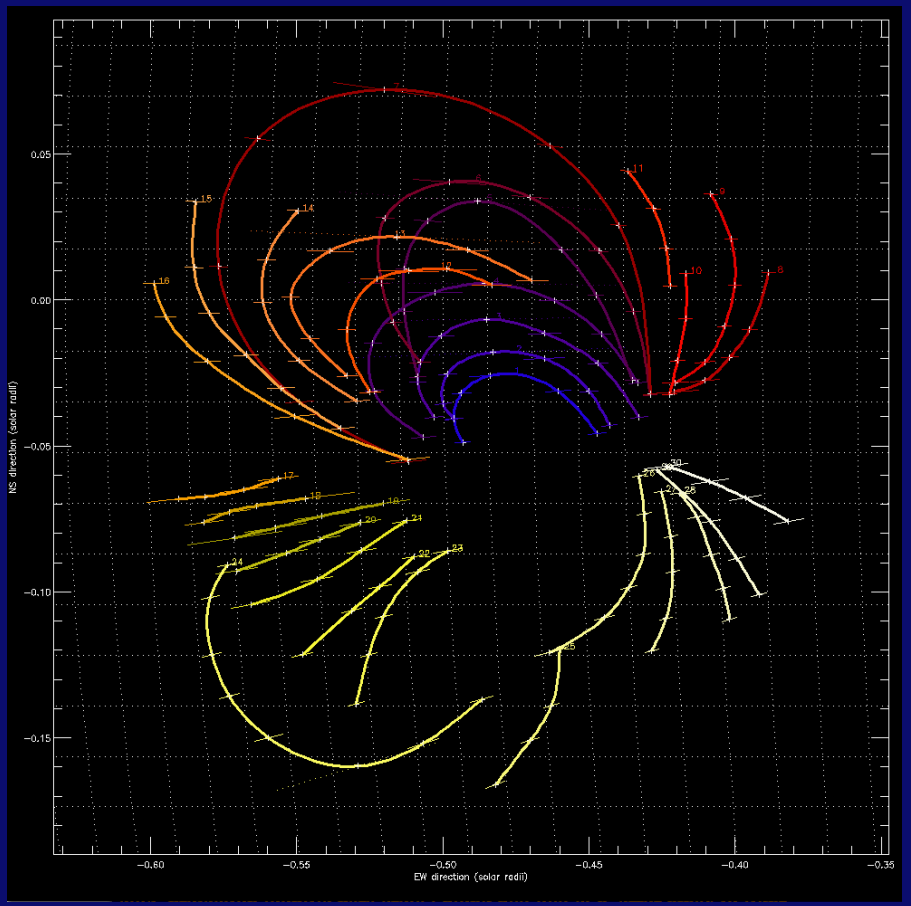

Entire loops are only visible because of the large inclination angles:

$\theta \sim 51 \ldots 73$ deg

so that their apex is in an altitude of less than about a hydrostatic scale height.

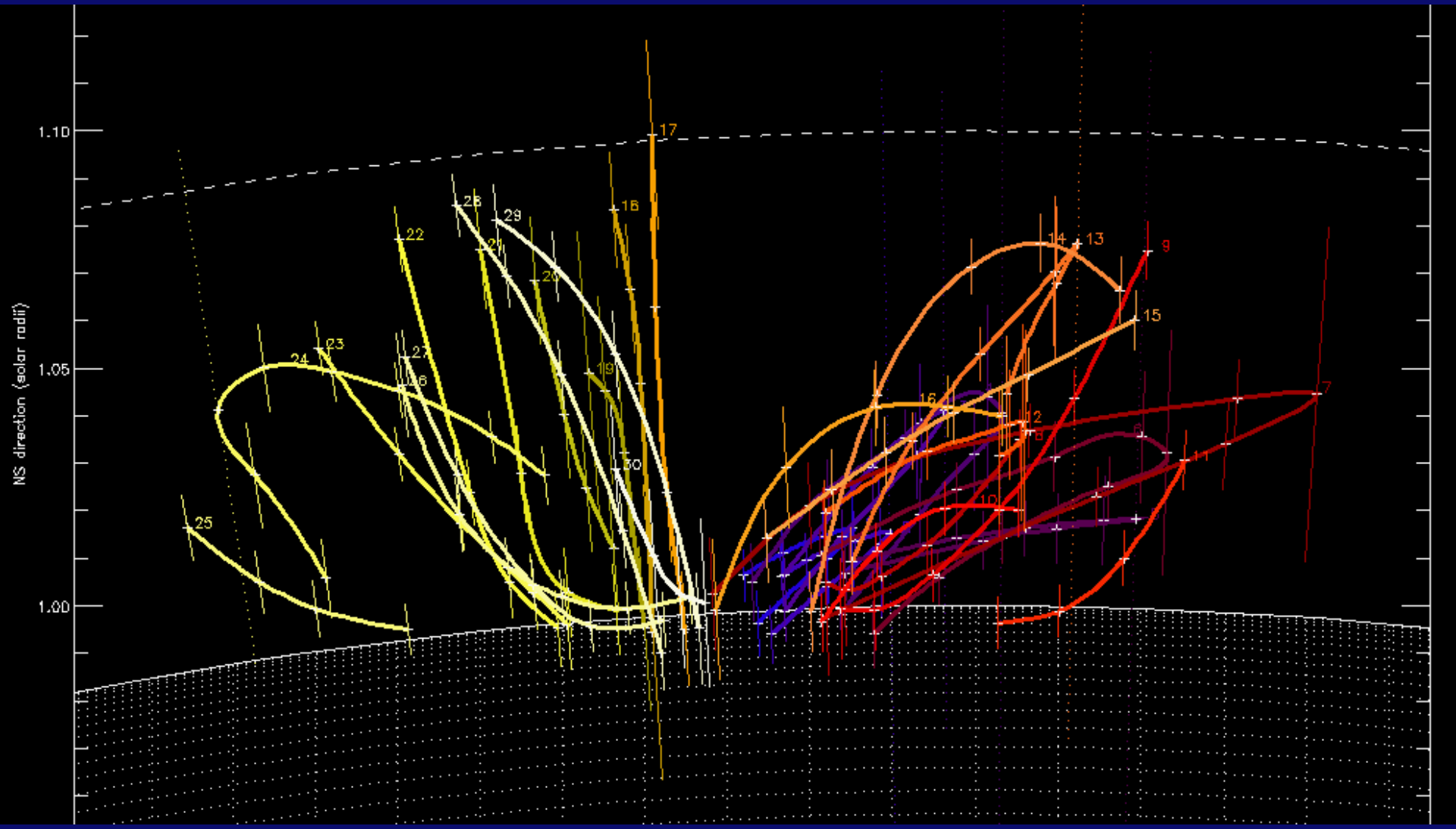

The height limit of detectable loops is given by the dynamic range of the (hydrostatic) emission measure contrast:

$$\frac{EM(h=h_{\max})}{EM(h=0)} = \exp(-\frac{h_{\max}}{\lambda_{EM}(T=1MK)}) = \exp(-\frac{70}{23}) \sim 0.05, \lambda_{EM} = \frac{1}{2}\lambda_n$$

Density and Temperature Measurements

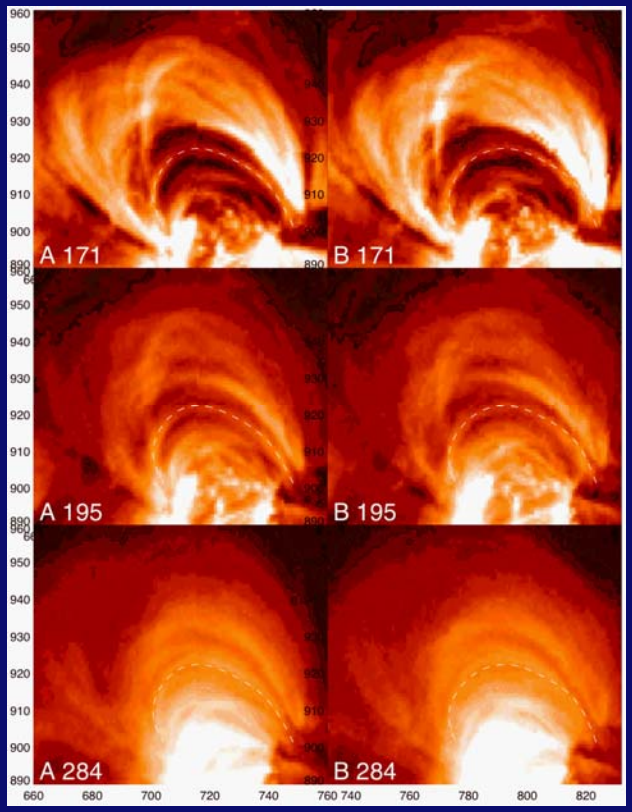

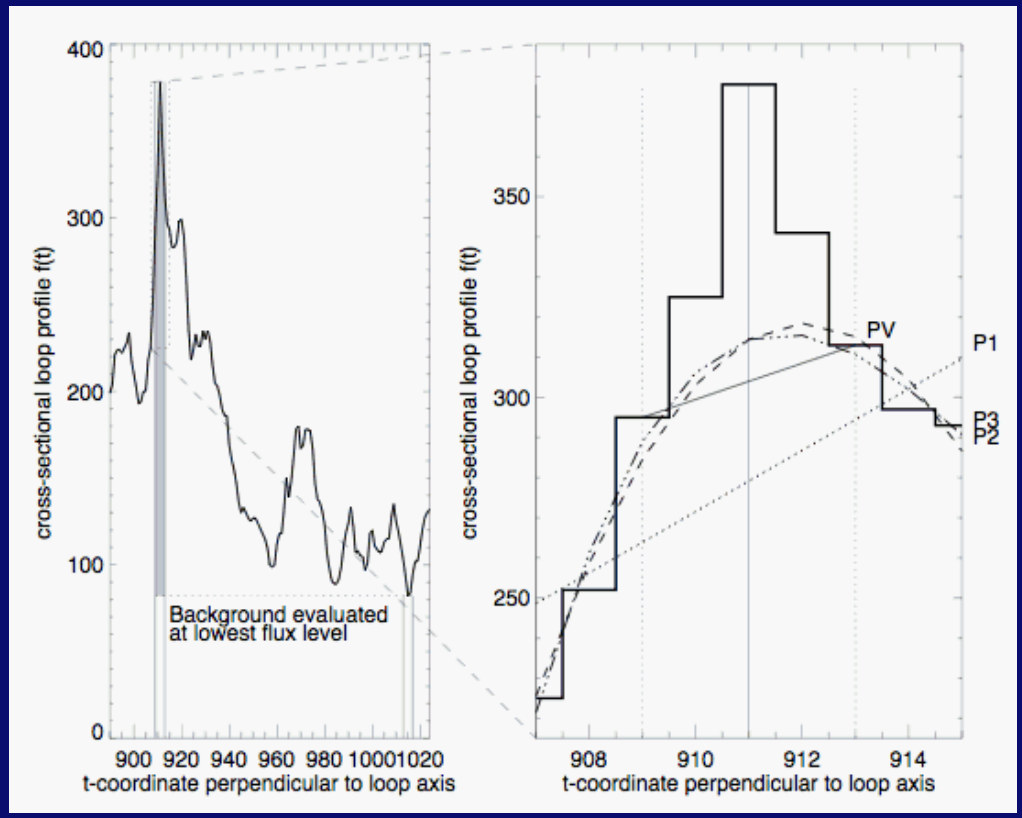

The determination of the density and temperature of a loop can only be done after background subtraction.
The finest loop strands have typically a loop-related EUV flux of < 10%, and thus suitable background modeling in all 3 temperature filters is required.

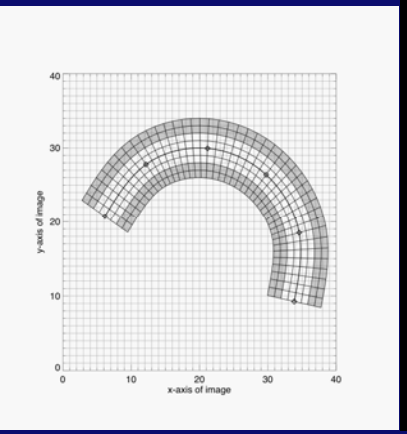

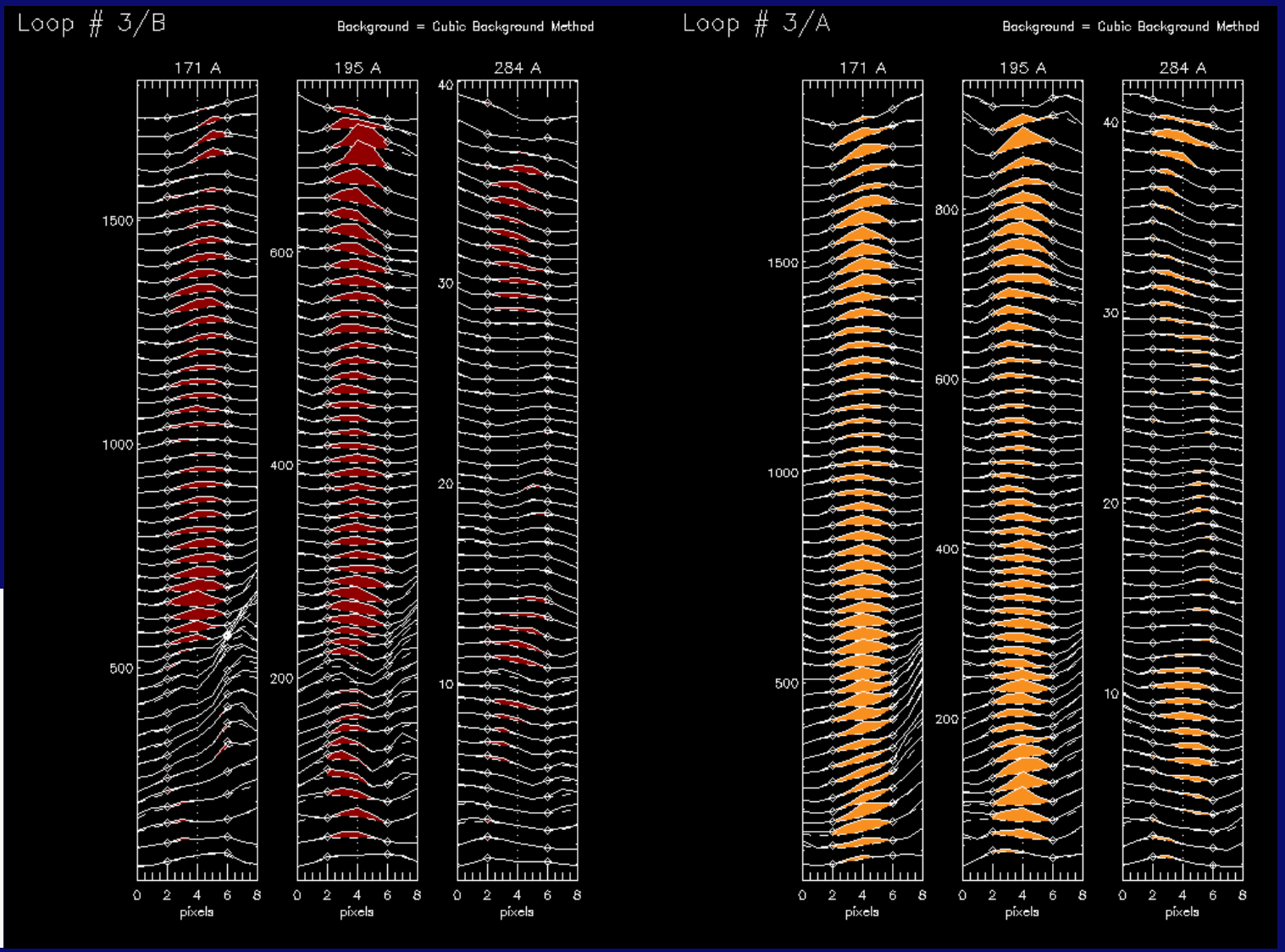

Loop cross-section profiles are extracted from image.
Background modeling with cubic polynomial interpolation.

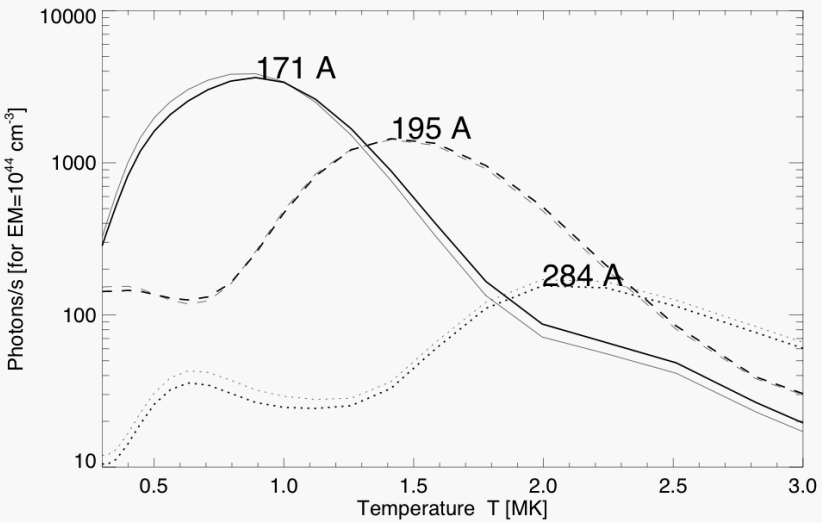

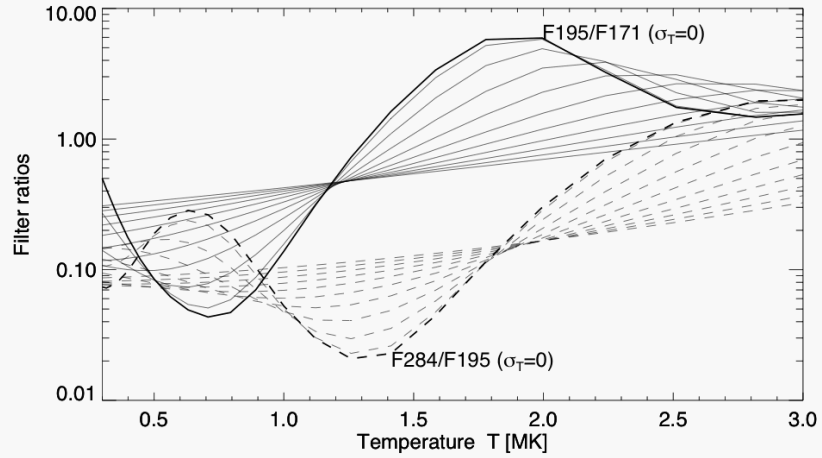

Temperature response functions of EUVI, A+B

Filter ratios for Gaussian DEM distributions:

$$\left(\frac{dEM(T)}{dT}\right)(s)dT = EM_p(s) * \exp\left(-\frac{[T - T_p(s)]^2}{2\sigma_{DEM}^2}\right)$$

$$[f_{171}(s) - b_{171}(s)] = \int \frac{dEM(T)}{dT}(s) R_{171}(T) dT$$

$$[f_{195}(s) - b_{195}(s)] = \int \frac{dEM(T)}{dT}(s) R_{195}(T) dT$$

$$[f_{284}(s) - b_{284}(s)] = \int \frac{dEM(T)}{dT}(s) R_{284}(T) dT$$

Triple-filter analysis:
forward-fitting of EM_p, T_p, σ_{DEM}:

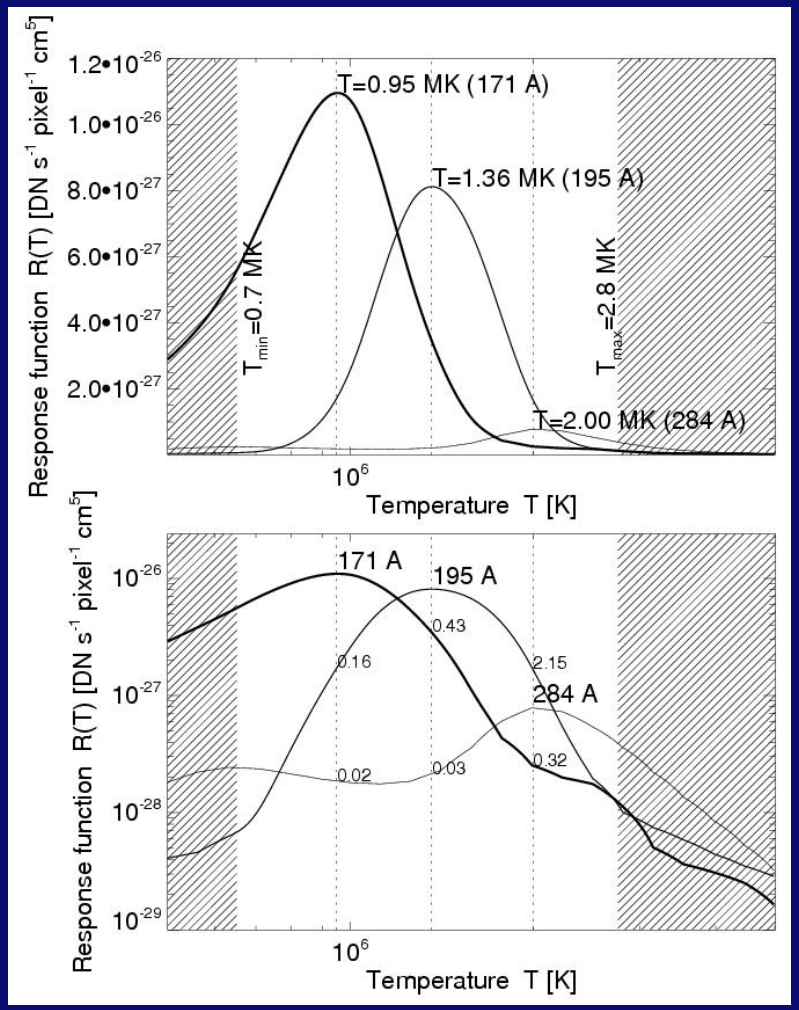

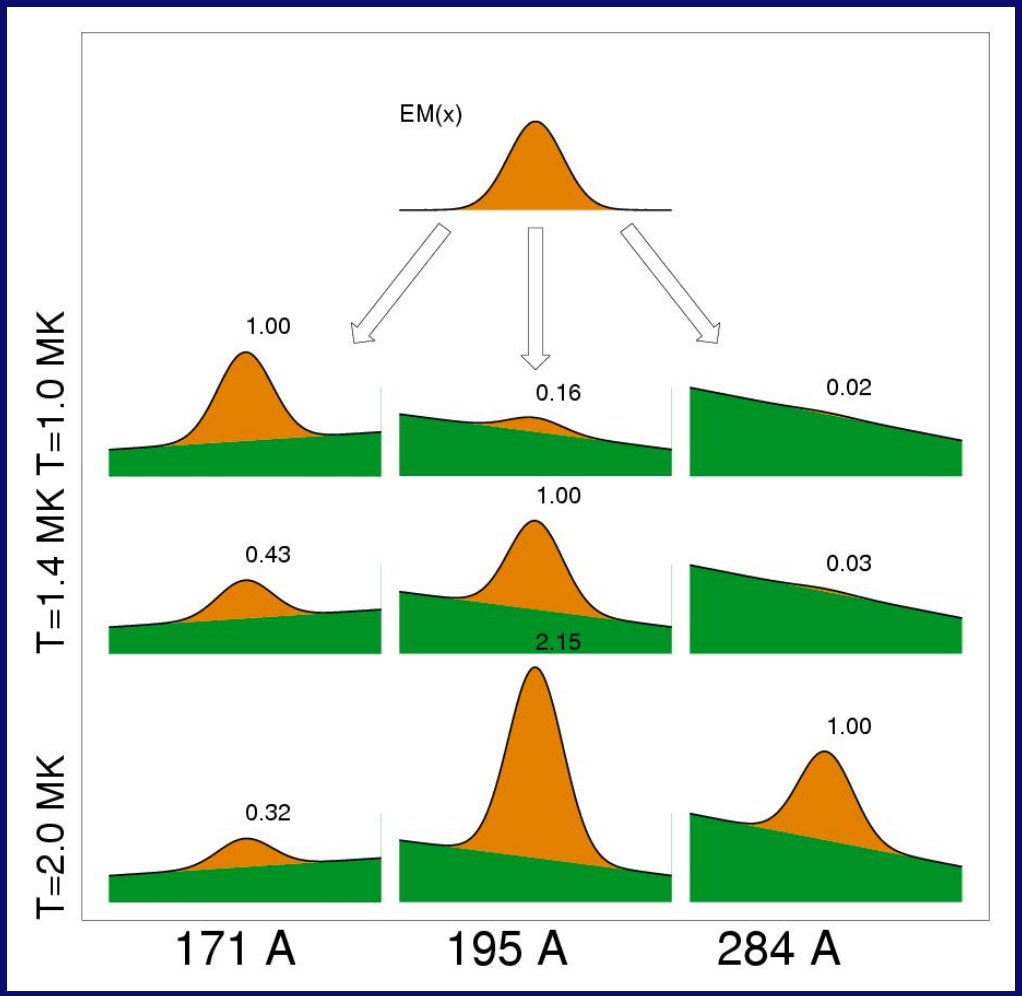

Example of simulating 3 iso-thermal (T_i=1.0, 1.4, 2.0 MK) loop cross-sections EM(x) with Gaussian profile, scaled with the TRACE response functions $R_w(T)$ that yields in each case the profiles $F_w(x)=EM(x) * R_w(T_i)$ seen in the three filters (w=171, 195, 284 A).

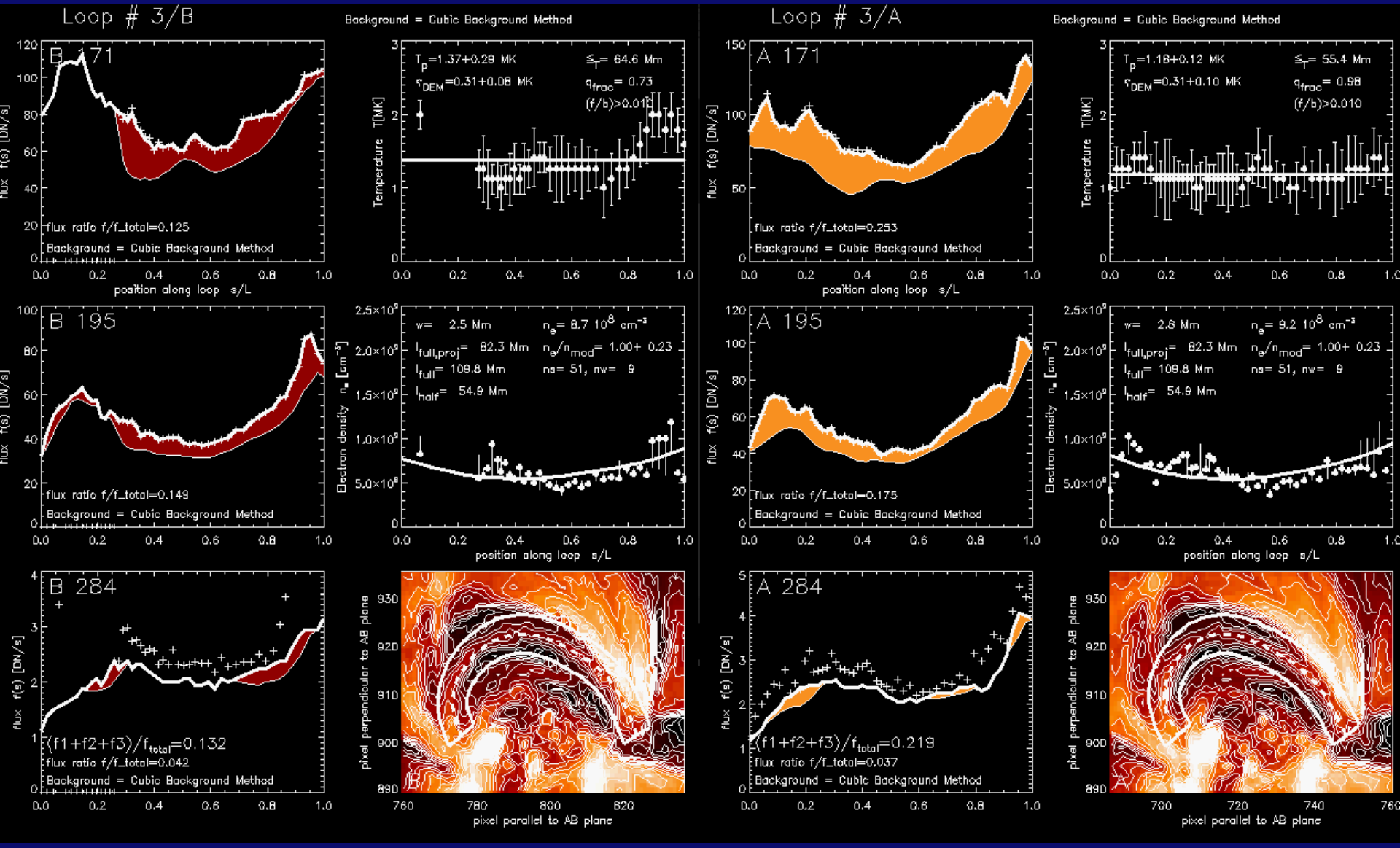

Input: background-subtracted loop flux profiles
Output: Electron density and temperature profiles

The advantage of STEREO is that a loop can be mapped from two different directions, which allows for two independent background subtractions. This provides an important consistency test of the loop identity and the accuracy of the background flux subtraction.

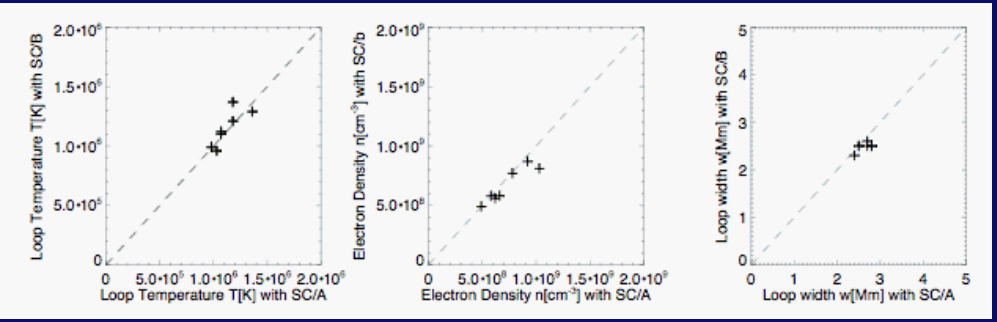

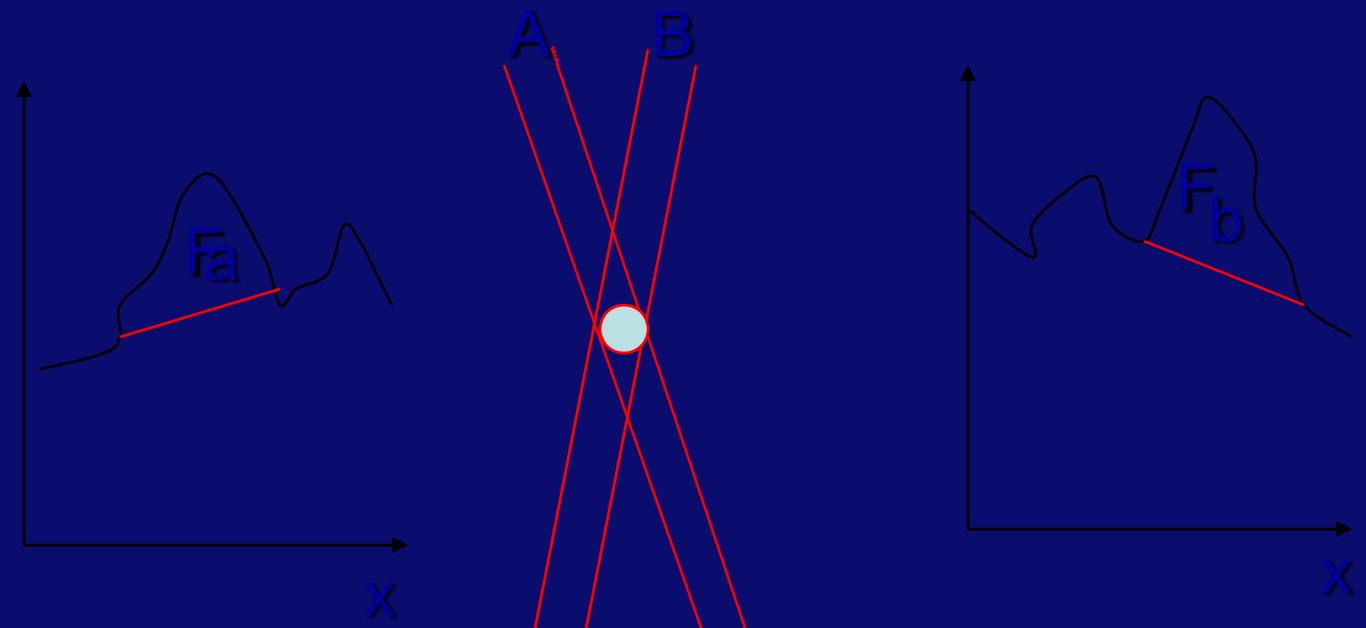

Consistency check: Is F_a = F_b ?

Consistency test between STEREO A+B:

Two independent background subtractions from identical loop seen from two different angles:

Do we arrive at the same loop widths, densities, and temperatures ?

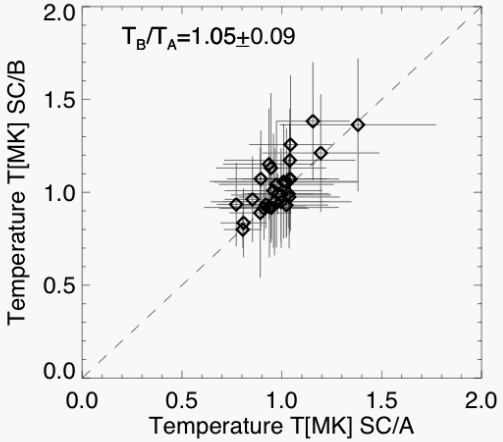

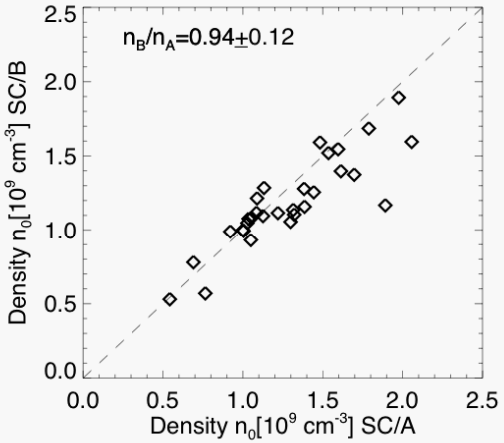

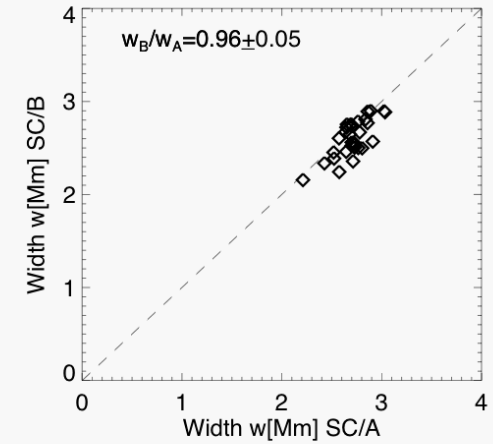

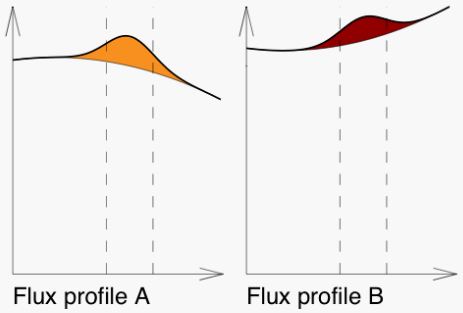

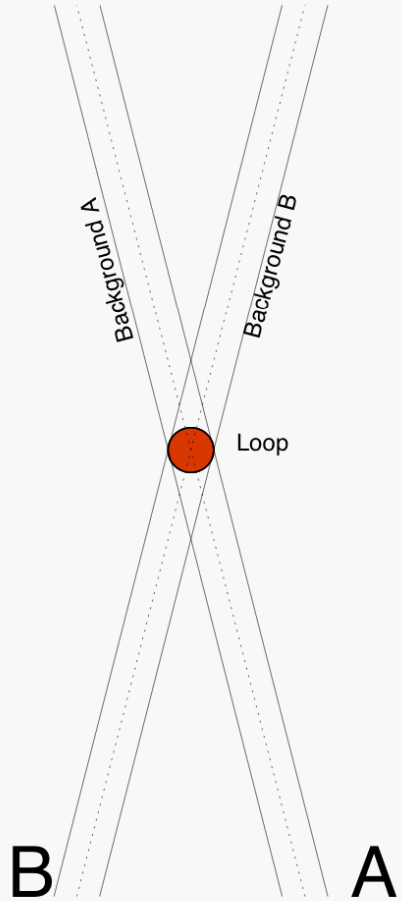

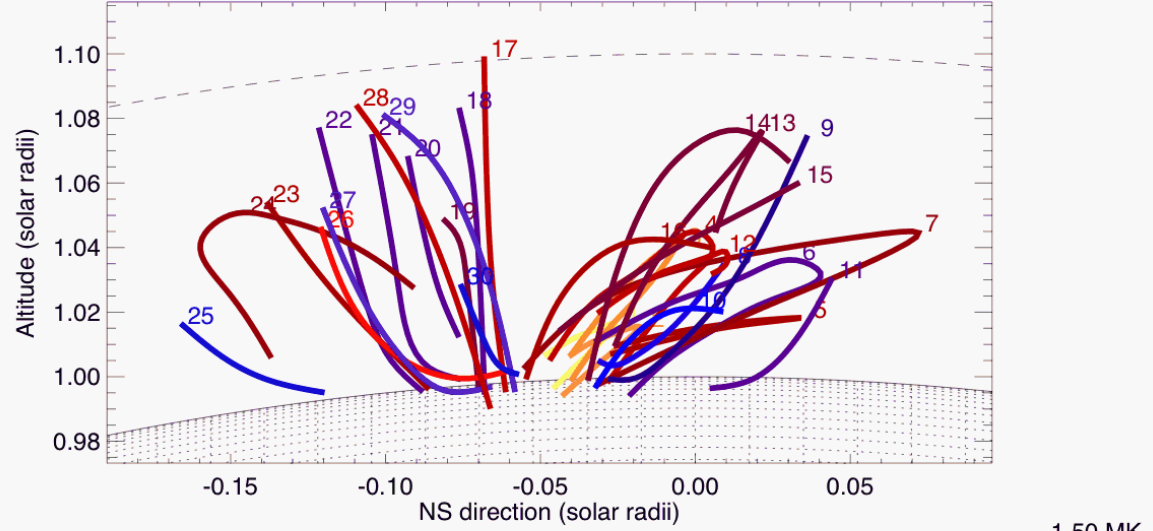

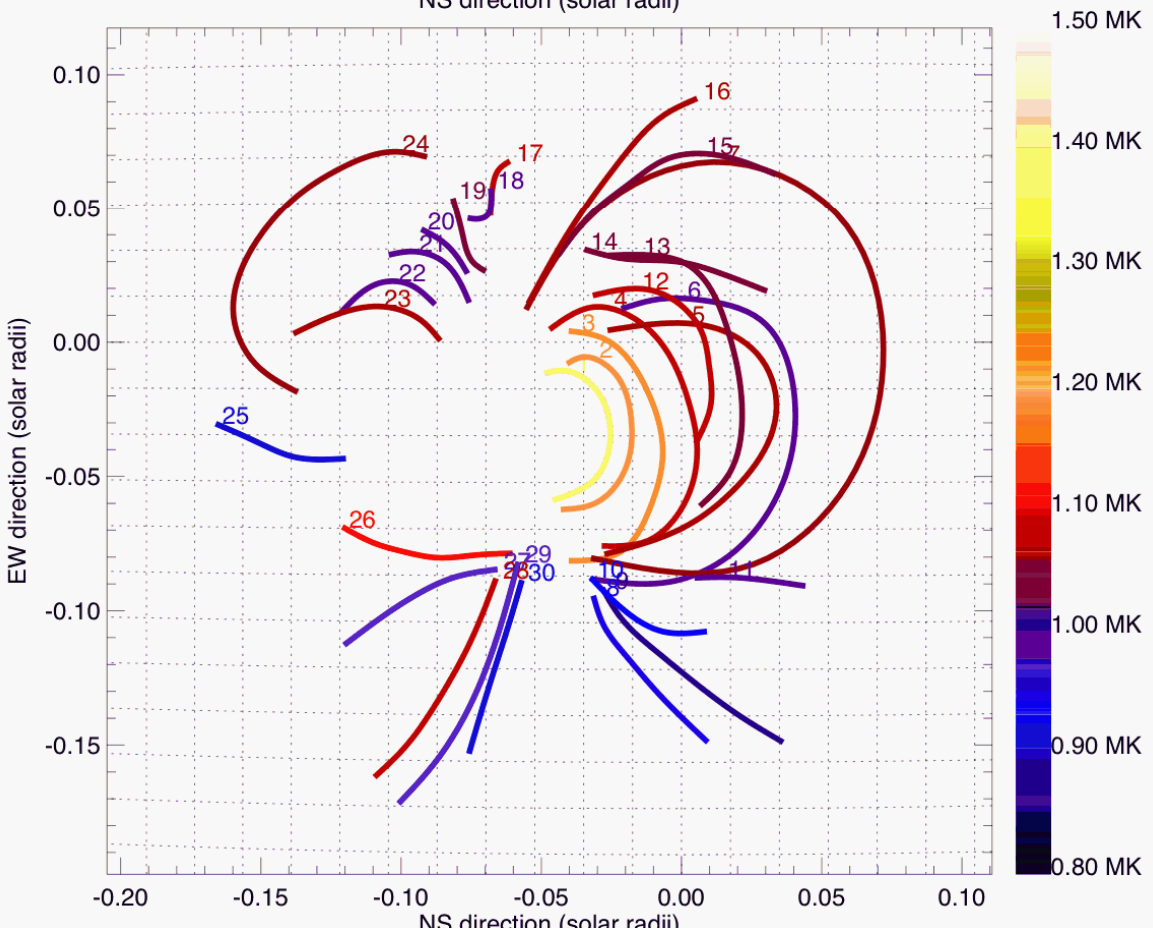

A colored temperature map of 30 loops with temperatures in the range of T=0.8-1.5 MK

The hottest loops tend to be the smallest loops, located in the center of the active region.

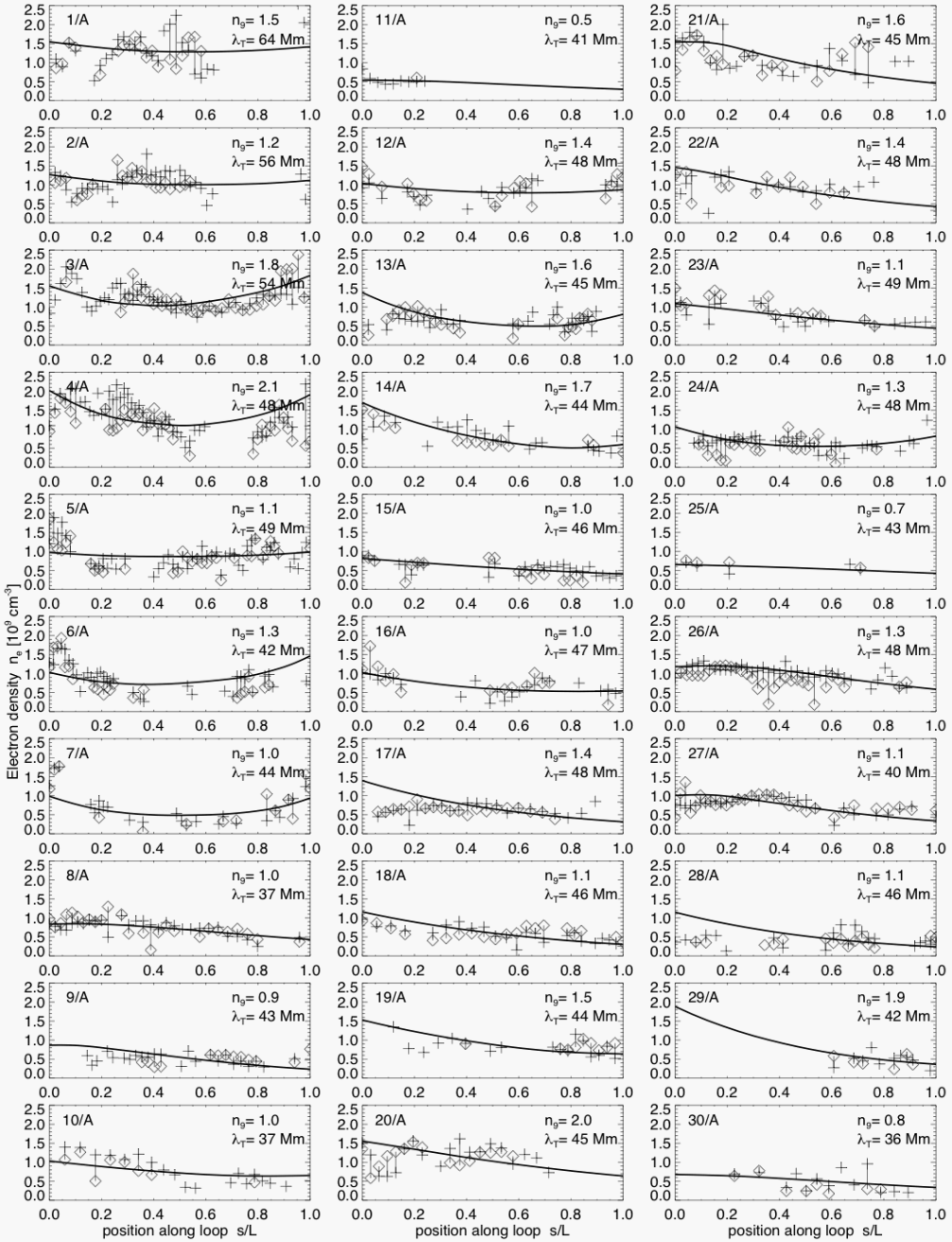

The density profiles n(h) are consistent with the gravitational stratification of hydrostatic loops,

$$n(h) = n_{base} \exp(-h/\lambda_T)$$

defined by the temperature scale heights λ_T and stereoscopically measured from the height profiles h(s).

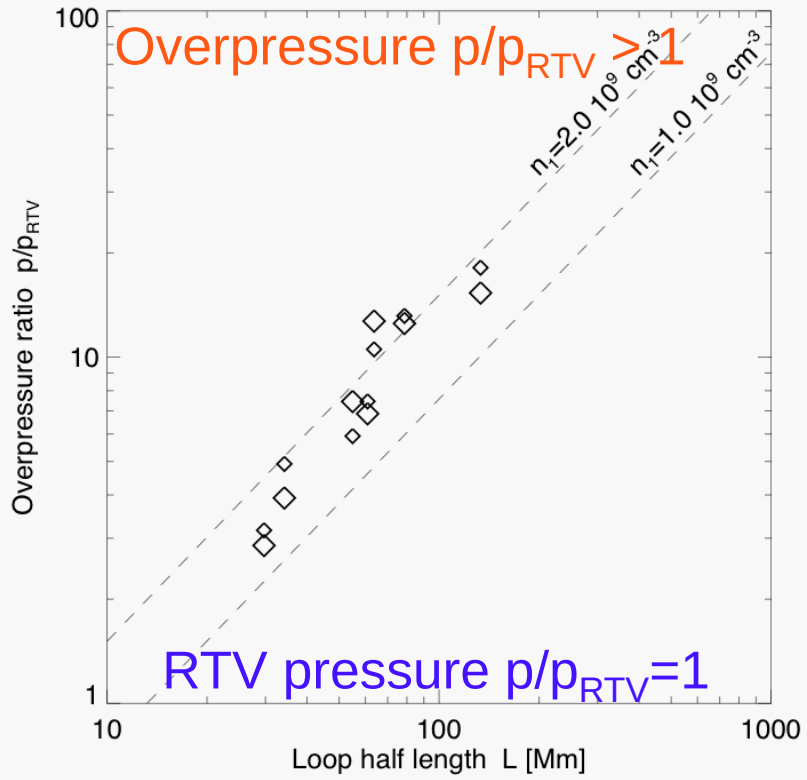

The observed densities are not consistent with hydrostatic equilibrium solutions, but rather display the typical overpressures of loops that have been previously heated to higher temperatures and cool down in a non-equilibrium state, similarly to earlier EIT and TRACE measurements.

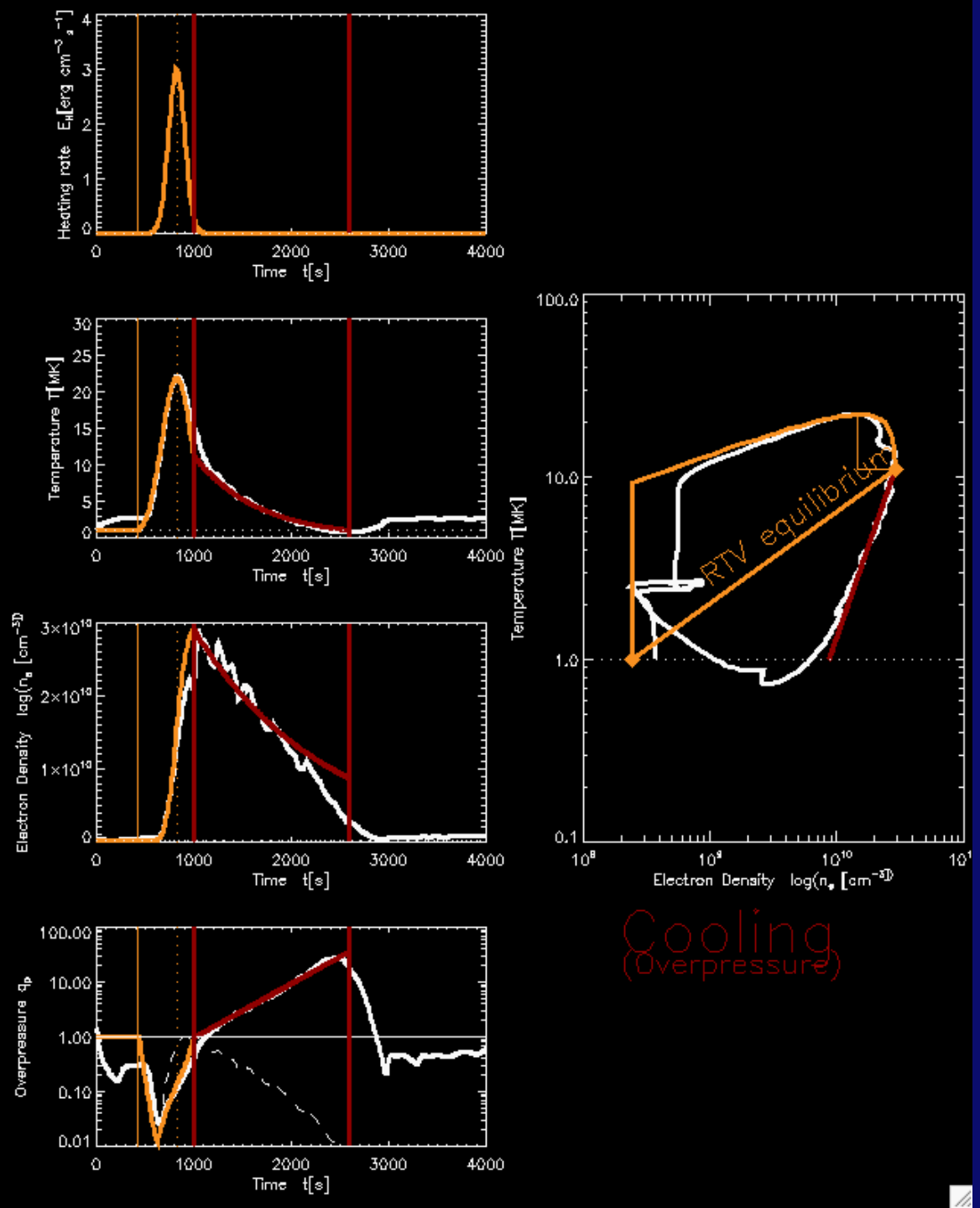

Hydrodynamic simulations of impulsively heated loops reveal :

(i) an underpressure (compared with the RTV hydrostatic equilibrium solution) during the heating phase,

(ii) an RTV (energy balance) equilibrium point at the density peak, and

(iii) an increasing overpressure during the cooling phase, approximately following the Jakmiec relation $T(t) \sim n(t)^2$

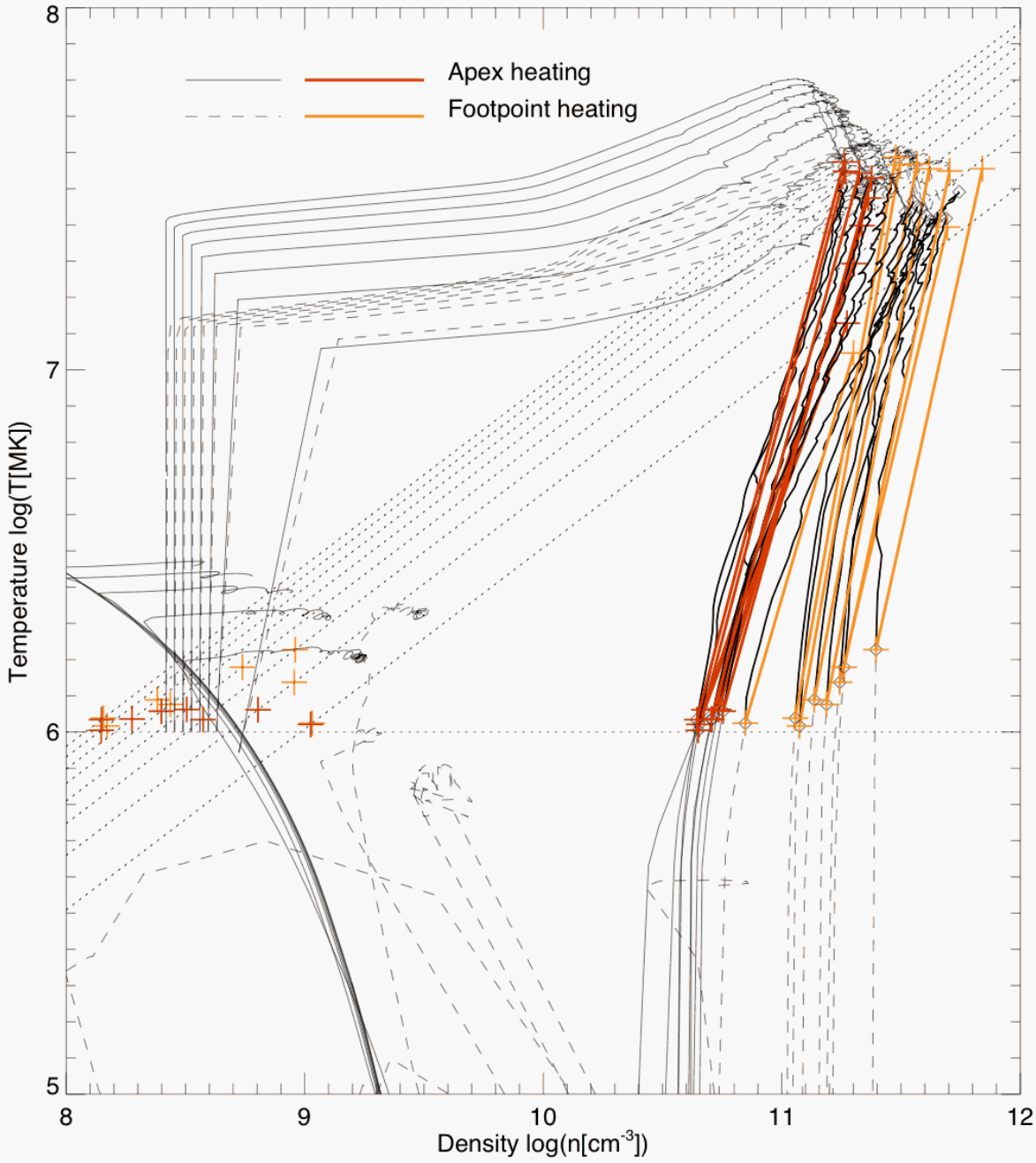
Apex heating
Footpoint heating
Temperature log(T[MK])
Density log(n[cm^{-3}])
8
7
6
5
8
9
10
11
12

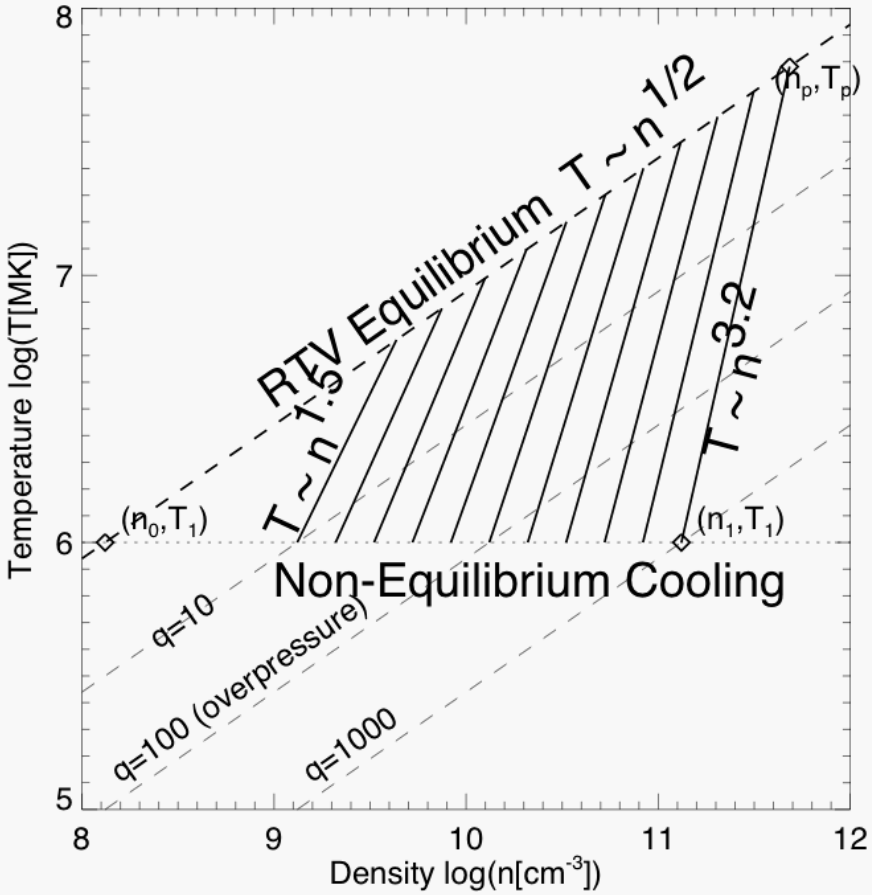

EUV loops are generally observed during the non-equilibrium cooling phase, where they exhibit a high overpressure. The previously hotter temperature during the heating phase can be detected in soft X-rays. (see Winebarger, Warren, & Mariska 2003).

Image Preprocessing: (3) Multi-filter loop tracing

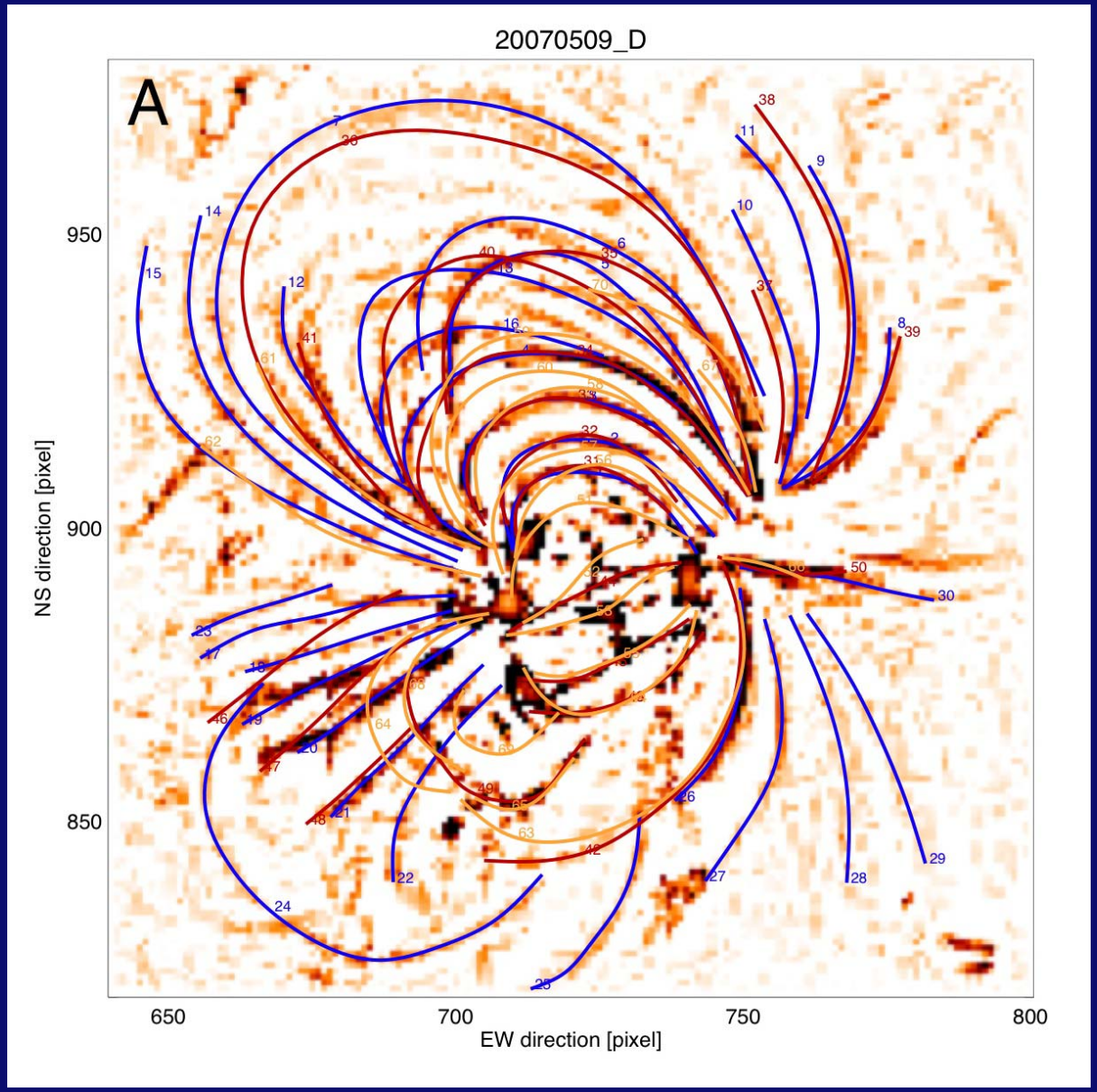

3D Reconstruction of 100 loops (T=1.0-2.0 MK)

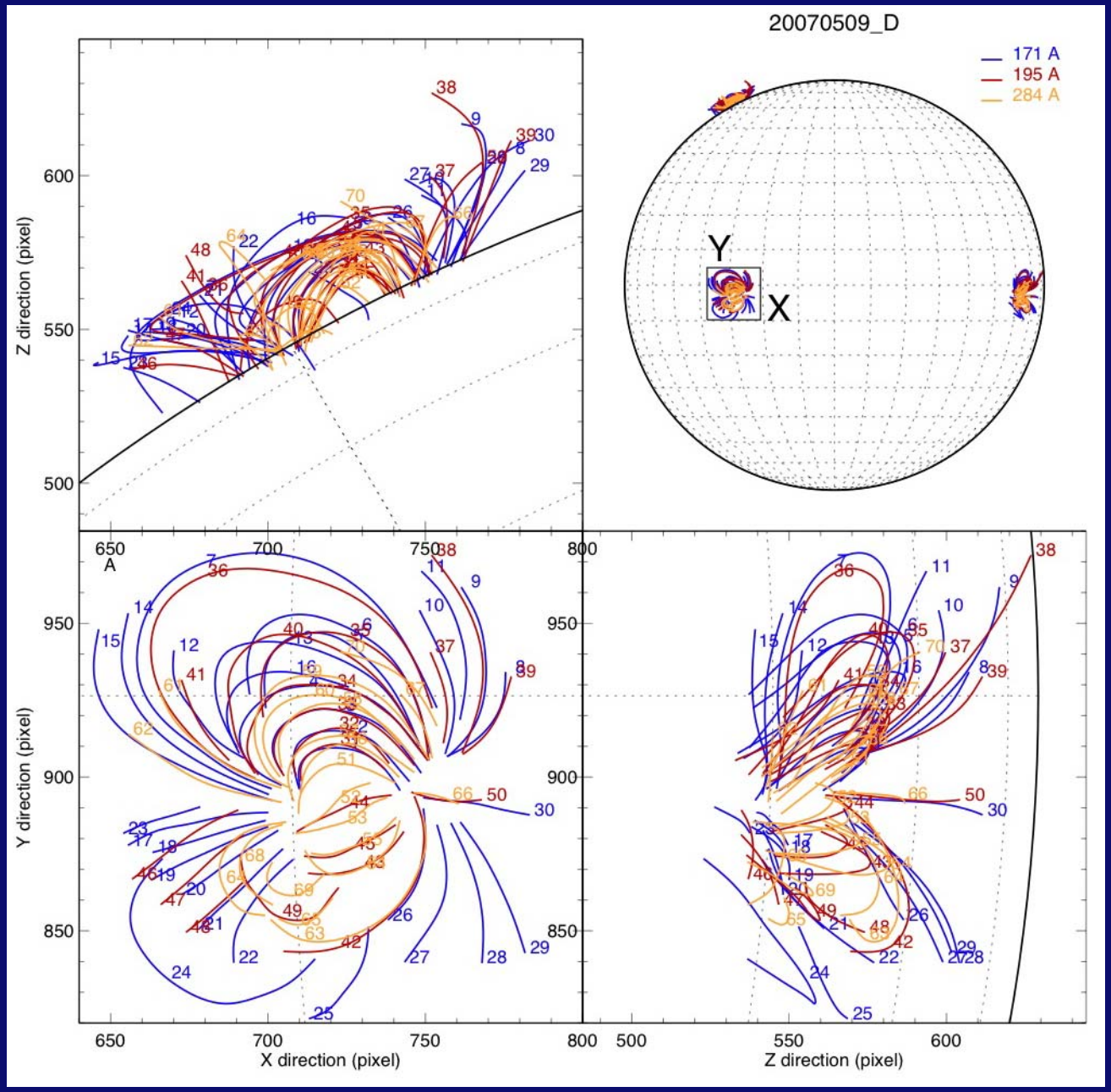

3D Field Interpolation

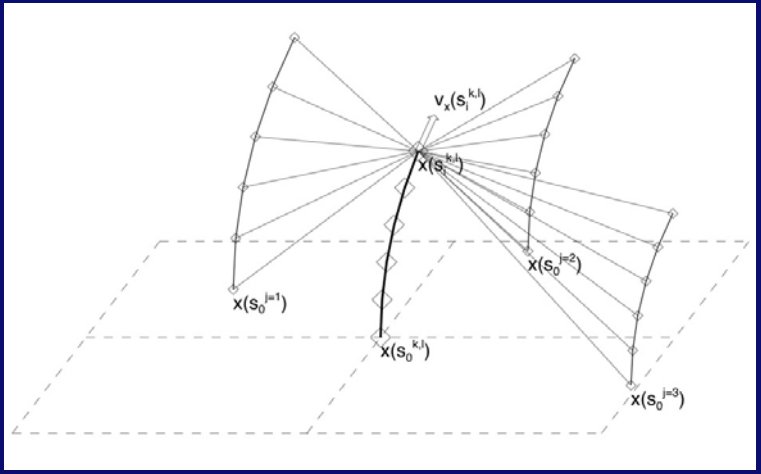

Skeleton field = triangulated 3D loops

3D field vector = weighted 3D-interpolation

In the following we describe our 3D field interpolation algorithm. The output of stereoscopic triangulation yields the 3D coordinates $[x(s_i), y(s_i), z(s_i)]$ as a function of the loop length coordinate $s_i, i = 1, ..., n_s^j$ for a set of $j = 1, ..., n_j$ loops. We define the normalized field direction vectors $\mathbf{v}(s_i)$ at every point s_i along a loop,

$$\begin{aligned} v_x(s_i) &= [x(s_{i+1}) - x(s_i)]/|v| \\ v_y(s_i) &= [y(s_{i+1}) - y(s_i)]/|v| \\ v_z(s_i) &= [z(s_{i+1}) - z(s_i)]/|v| \ , \end{aligned} \tag{3}$$

which are normalized to a length of unity by dividing with the length $|v(s_{i+1}) - v(s_i)|$ of the directional vector v_i,

$$|v| = \sqrt{[x(s_{i+1}) - x(s_i)]^2 + [y(s_{i+1}) - y(s_i)]^2 + [z(s_{i+1}) - z(s_i)]^2} \ . \tag{4}$$

These vectors $\mathbf{v}_i^j$ defined for each loop length coordinate $s_i, i = 1, ..., n_s^j$ and loop $j = 1, ..., n_j$ form the skeleton field of our field line interpolation scheme. We can now compute a new set of field lines $x(s_i^{k,l}), y(s_i^{k,l}), z(s_i^{k,l})]$ starting in a 2D-cartesian grid of footpoints k, l that covers the solar surface at the lower boundary of the 3D interpolation box with height range $h = [0, h_{max}]$. A new field line starts at a given footpoint position $[x(s_1^{k,l}), y(s_1^{k,l}), z(s_1^{k,l})]$ and is iteratively computed along the loop length coordinate $s_i^{k,l}$ by interpolating the field direction $\mathbf{v}(s_i^{k,l})$ at position $[x(s_i^{k,l}), y(s_i^{k,l}), z(s_i^{k,l})]$ (as illustrated in Fig. 5),

$$\begin{aligned} v_x(s_i^{k,l}) &= \sum_m [v_x(s_m) w(s_m) p(s_m)] / \sum_m w(s_m) \\ v_y(s_i^{k,l}) &= \sum_m [v_y(s_m) w(s_m) p(s_m)] / \sum_m w(s_m) \\ v_z(s_i^{k,l}) &= \sum_m [v_z(s_m) w(s_m) p(s_m)] / \sum_m w(s_m) \ , \end{aligned} \tag{5}$$

where the index m runs over all n_s^j old loop length coordinates $s_i, i = 0, ..., n_s^j$ of all $j = 1, ..., n_j$ loops. The factor $w(s_m)$ is a weighting factor of the skeleton vector $\mathbf{v}(s_m)$ that decreases quadratically with distance,

$$w(s_m) = \left(\sqrt{[x(s_m) - x(s_i^{k,l})]^2 + [y(s_m) - y(s_i^{k,l})]^2 + [z(s_m) - z(s_i^{k,l})]^2} \right)^{-2} \ , \tag{6}$$

which ensures that those skeleton field lines have the highest weight that are closest to the interpolation location. The coordinate of the next position $s_{i+1}^{k,l}$ of the new loop is then defined by

$$\begin{aligned} x(s_{i+1}^{k,l}) &= x(s_i^{k,l}) + v_x(x_i^{k,l})/|v| \\ y(s_{i+1}^{k,l}) &= y(s_i^{k,l}) + v_y(y_i^{k,l})/|v| \\ z(s_{i+1}^{k,l}) &= z(s_i^{k,l}) + v_z(z_i^{k,l})/|v| \ , \end{aligned} \tag{7}$$

where $|v|$ is the length of the field direction vector given in Eq. (5).

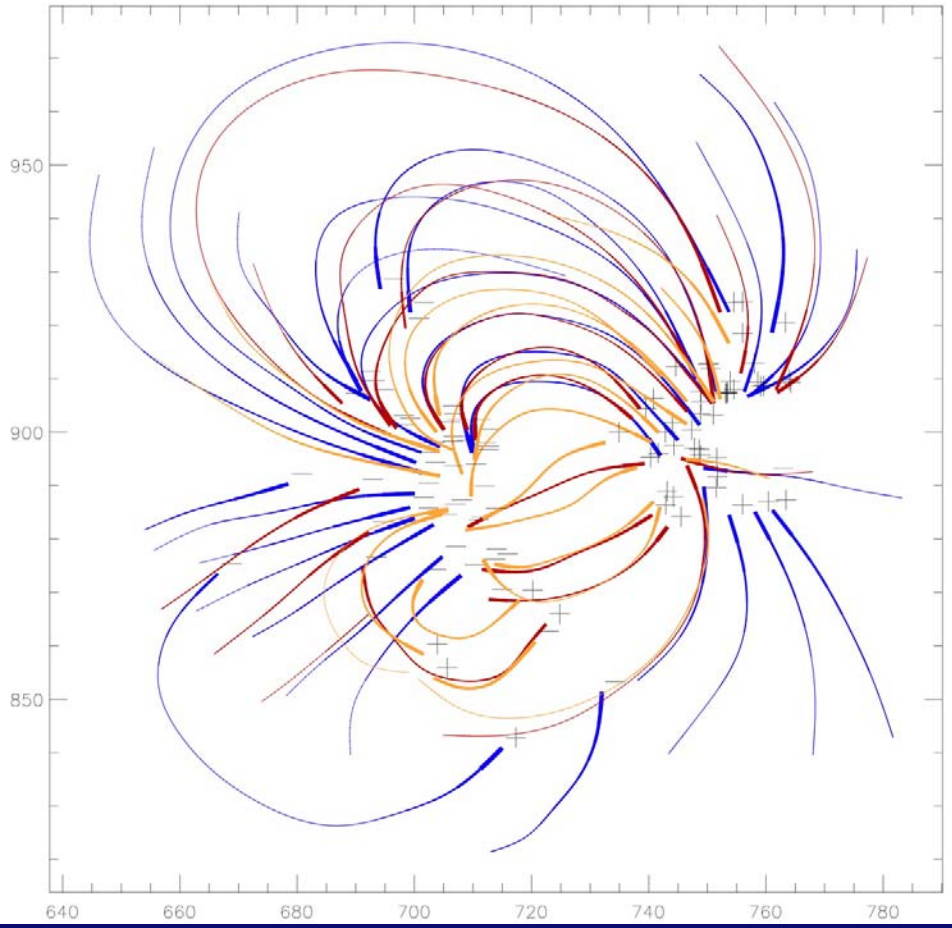

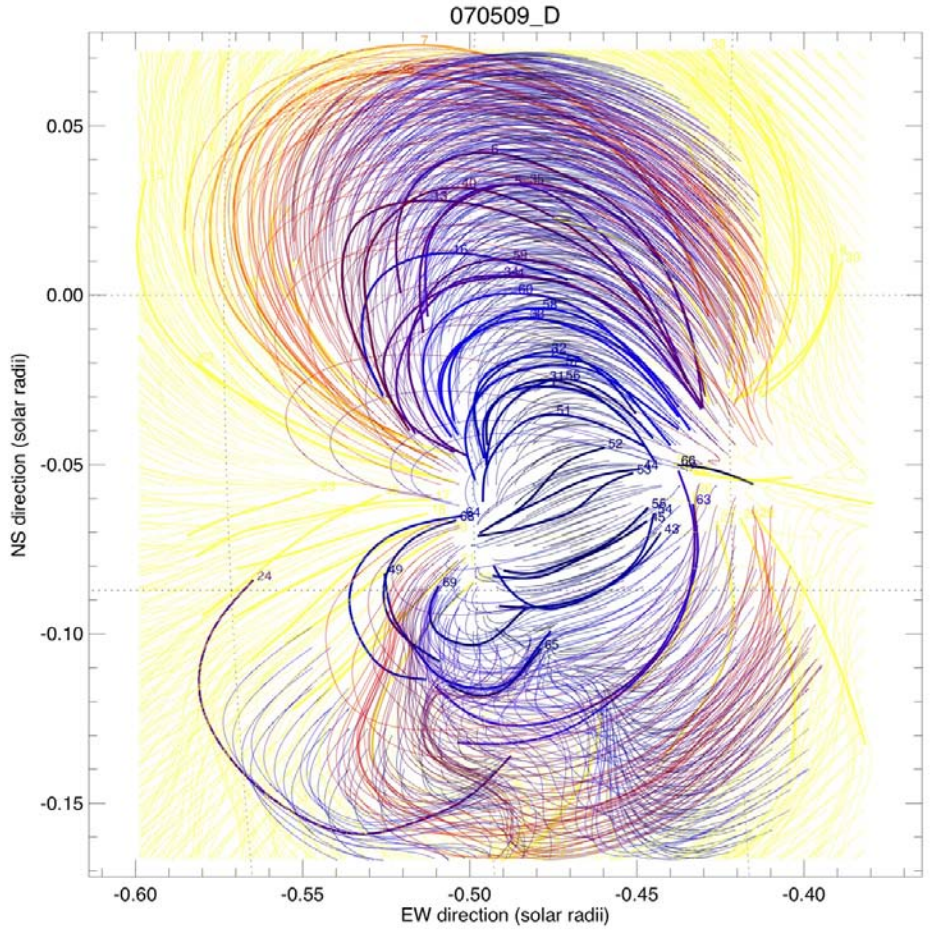

Skeleton field of 100 triangulated loops with polarity assignment according to proximity to photospheric dipole config.

3D field interpolation

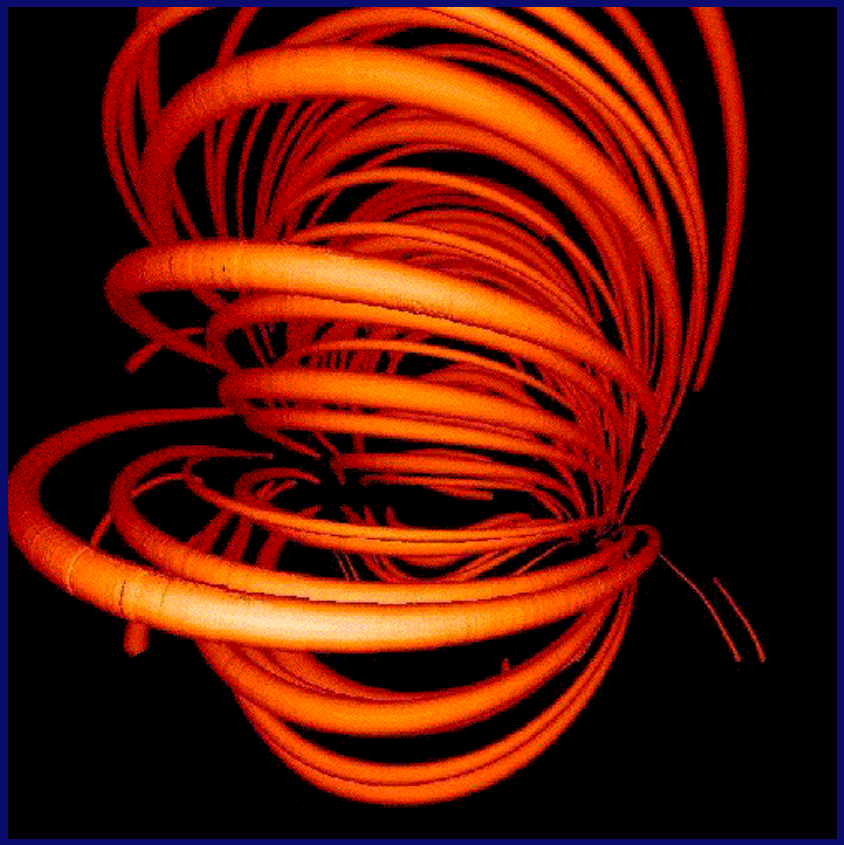

Tomographic volume rendering

For the physical parameterization of a 1-D loop density model we define pressure profiles $p(s)$ that decrease exponentially with height. Since many loops are asymmetric, we use two different base pressures (p_1, p_2), and two pressure scale heights (λ_1, λ_2), but the pressures have to match at the looptop, which constrains the pressure p_2 at the second footpoint as a function of the other parameters. The height $h(s)$ (vertical to the solar surface) as a function of the loop coordinate s is defined by the stereoscopically constrained 3D coordinates $s(x, y, z)$. So, the two half sides of a loop have the following pressure functions,

$$p(s < s_{top}, h \geq h_1) = p_1 \ \exp\left[-\frac{h(s) - h_{chr}}{\lambda_1}\right] , \tag{8}$$

$$p(s > s_{top}, h \geq h_2) = p_2 \ \exp\left[-\frac{h(s) - h_{chr}}{\lambda_2}\right] , \tag{9}$$

where the pressure p_2 is constrained by the matching condition at the looptop,

$$p(s = s_{top}) = p_1 \ \exp\left[-\frac{h_{top} - h_{chr}}{\lambda_1}\right] = p_2 \ \exp\left[-\frac{h_{top} - h_{chr}}{\lambda_2}\right] , \tag{10}$$

with an assumed chromospheric height of $h_{chr} = 2$ Mm. The coronal height range of both footpoints is located at the top of the chromosphere, so $h_1 \gtrsim h_{chr}$ and $h_2 \gtrsim h_{chr}$, but it can be somewhat higher in the transition region in the case of dynamic chromospheric processes.

For the parameterization of the temperature profile $T_e(s)$ we use the function

$$T_e(s) = T_{chr} + (T_m - T_{chr}) \left[\left(\frac{s - h_{chr}}{L - h_{chr}}\right)\left(2 - \frac{s - h_{chr}}{L - h_{chr}}\right)\right]^{2/7} , \tag{11}$$

which is a good approximation to hydrostatic temperature profiles for most uniform and non-uniform heating models (Aschwanden & Tsiklauri 2008). The temperature at the looptop (apex) is $T_e(s = s_{top}) = T_m$, if we define the loop half length by $L = s_{top}$, while the temperature at the footpoints drops to $T_e(s = h_{chr}) = T_e(s = 2L - h_{chr}) = T_{chr} \approx 10^4$ K. This functional form of the loop temperature profile seems generally closely to fit the observed EUV loops, regardless whether they are in a state of hydrostatic equilibrium or non-equilibrium, as model fits to single loop threads at highest spatial resolution demonstrate (e.g., Fig.5 in Aschwanden et al. 2000).

The electron density profile $n_e(s)$ is then simply defined by the relation for ideal gas as function of the pressure $p(s)$ and temperature $T_e(s)$,

$$n_e(s) = \frac{p(s)}{2k_B T_e(s)} , \tag{12}$$

with k_B being the Boltzmann constant.

The emission measure profile per voxel (with constant cross-section w_{loop}^2 and incremental length ds) is then,

$$dEM(s) = n_e^2(s) dV \approx n_e^2(s) w_{loop}^2 ds . \tag{13}$$

The flux profile $F_f(s)$ in a given filter wavelength f (171, 195, or 284 Å) is then defined (for a fully resolving instrument) by convolving the emission measure profile $EM(s)$ with the instrumental response function $R_f(T)$, which is a function of the loop temperature profile $T_e(s)$,

$$F_f(s) = \int EM(s) R_f(T[s]) ds . \tag{14}$$

For a realistic instrument with a point spread function width of w_{res} (i.e. 2.2 pixels for EUVI) and resolved loop width w_{loop}, the image of an observed loop has to be simulated by a convolution with a Gaussian kernel with the widths added in quadrature,

$$w_{obs} = \sqrt{w_{res}^2 + w_{loop}^2} . \tag{15}$$

Observations:
3 filter images

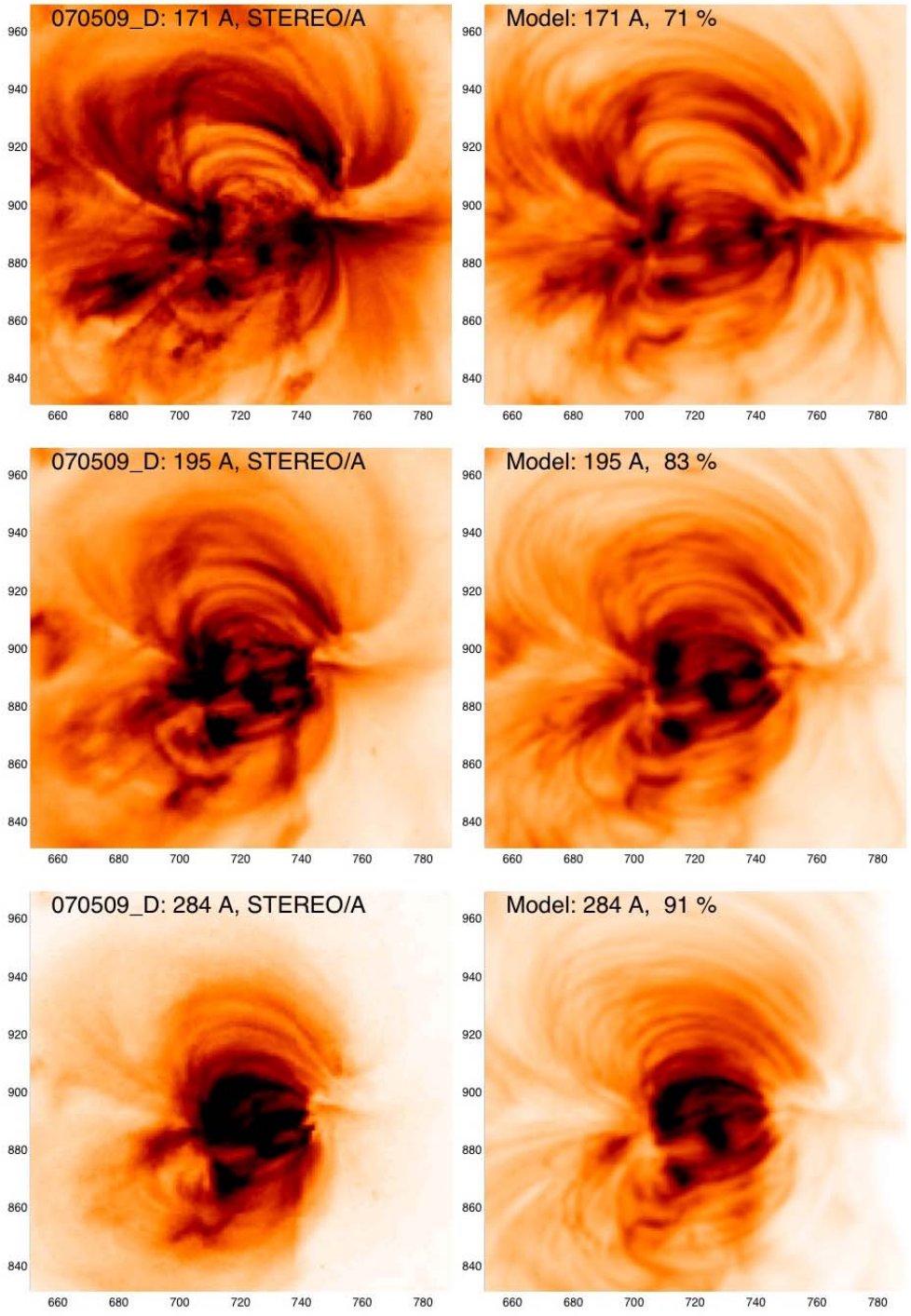

Model:
~7000 loops
(forward-fitting
of fluxes)

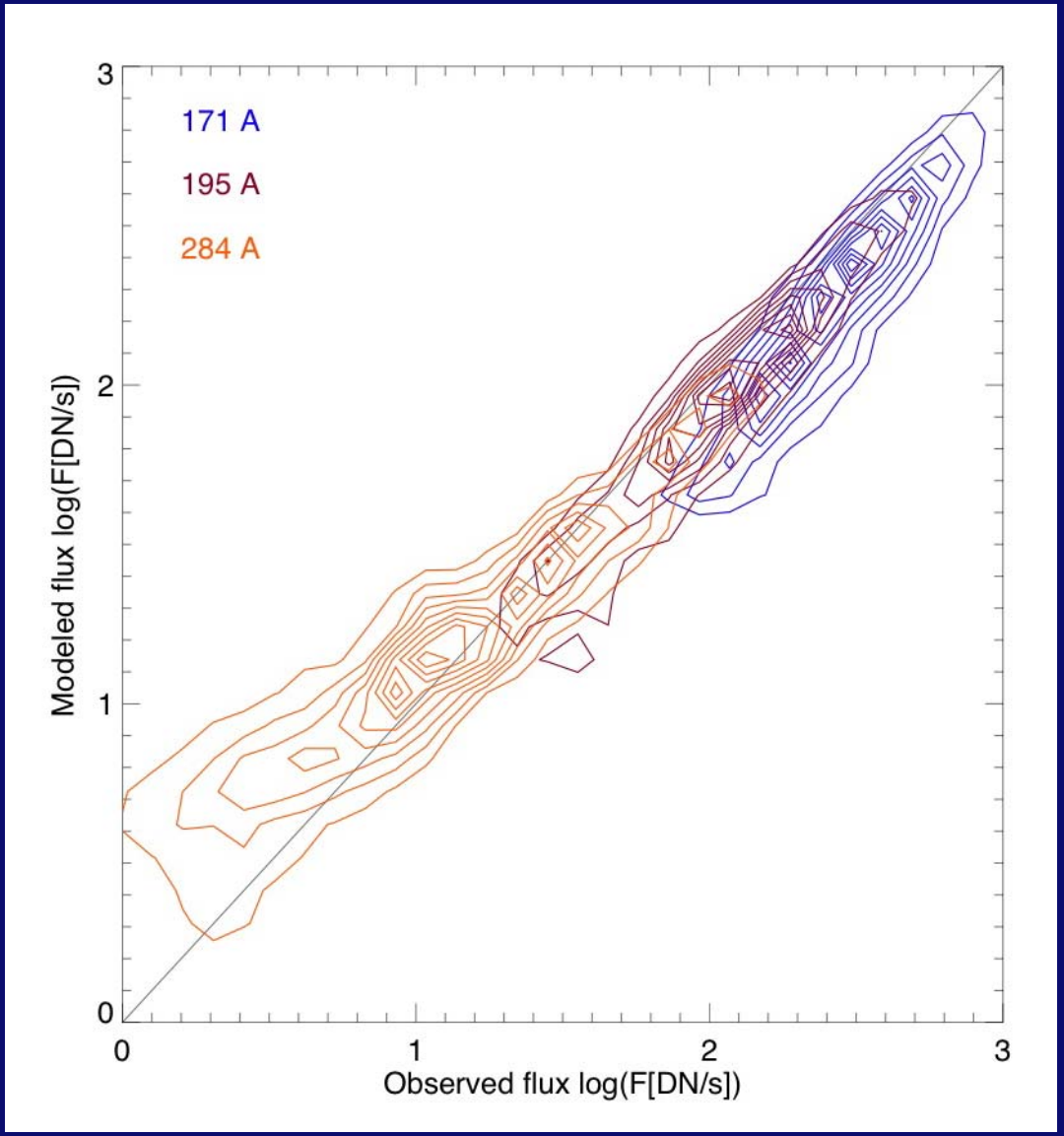

Consistency of modeled (forward-fitted) vs. observed fluxes

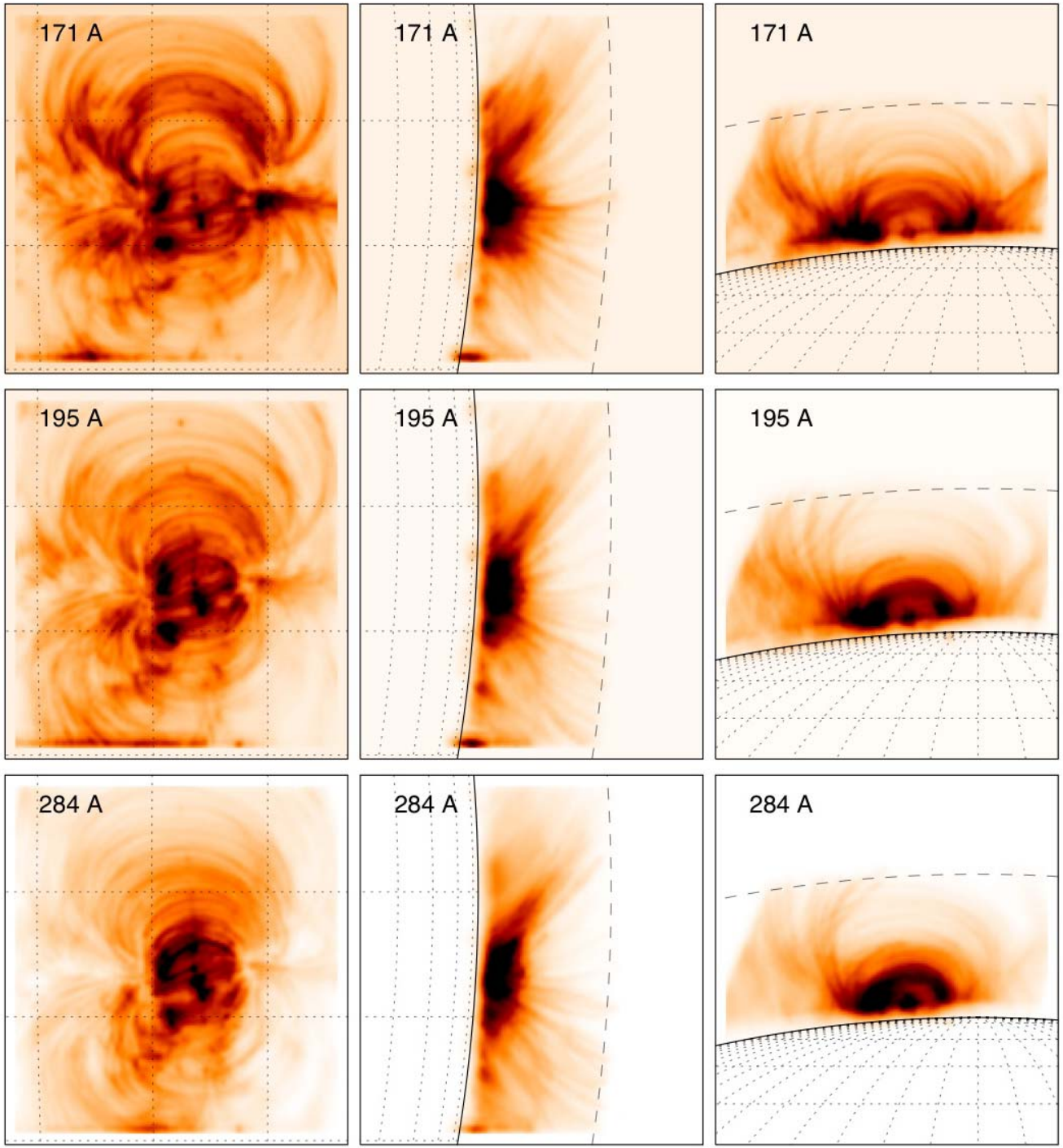

3 different views

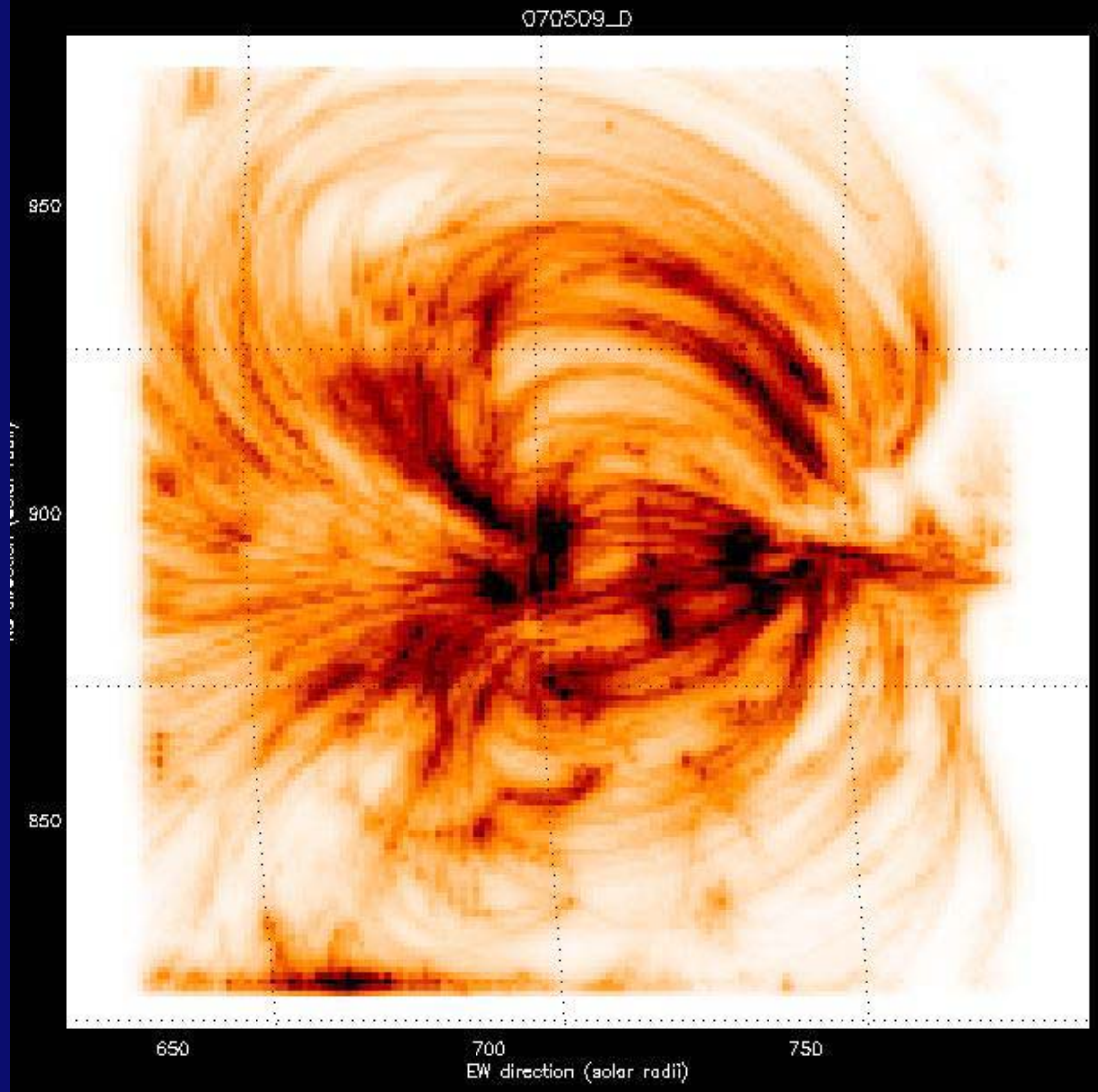
070509_D
950
900
850
650
700
750
EW direction (solar radii)

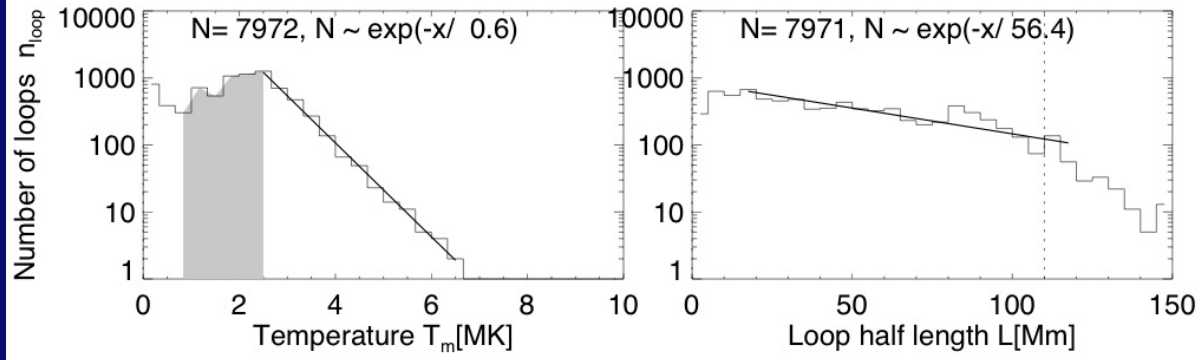

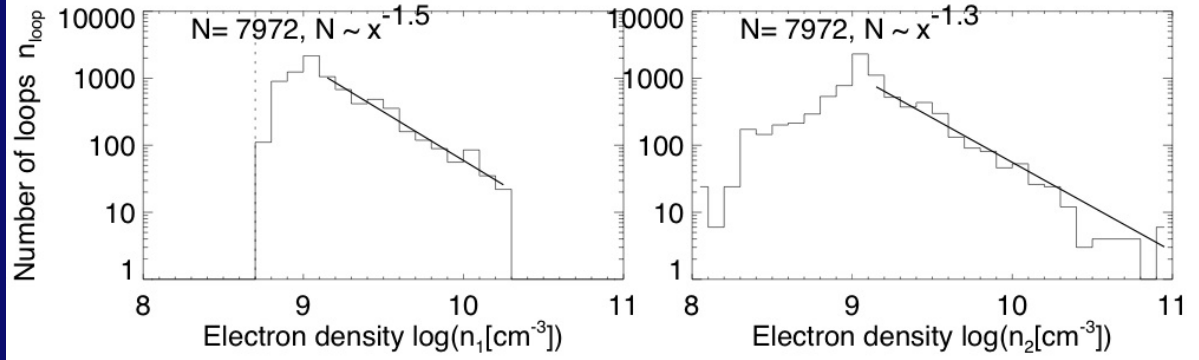

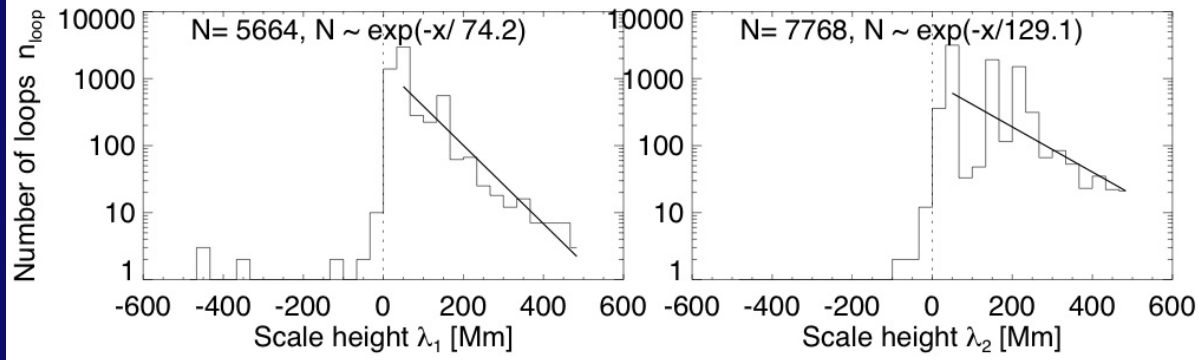

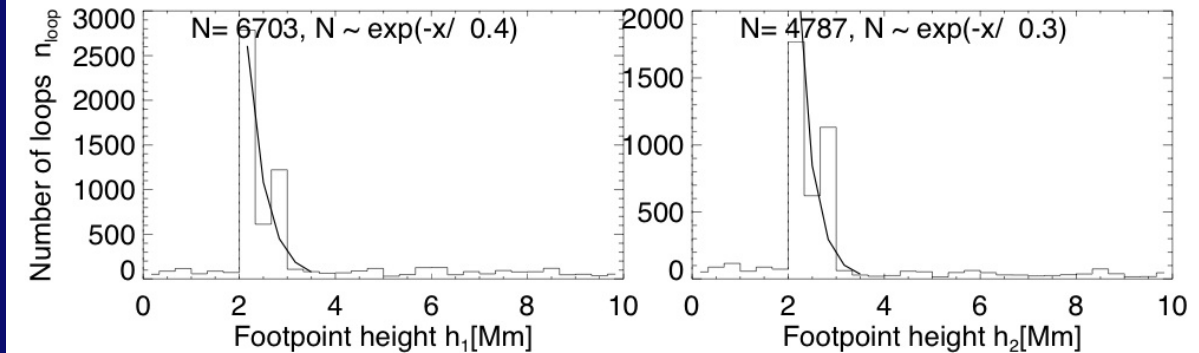

Statistical distributions of forward-fitted physical parameters

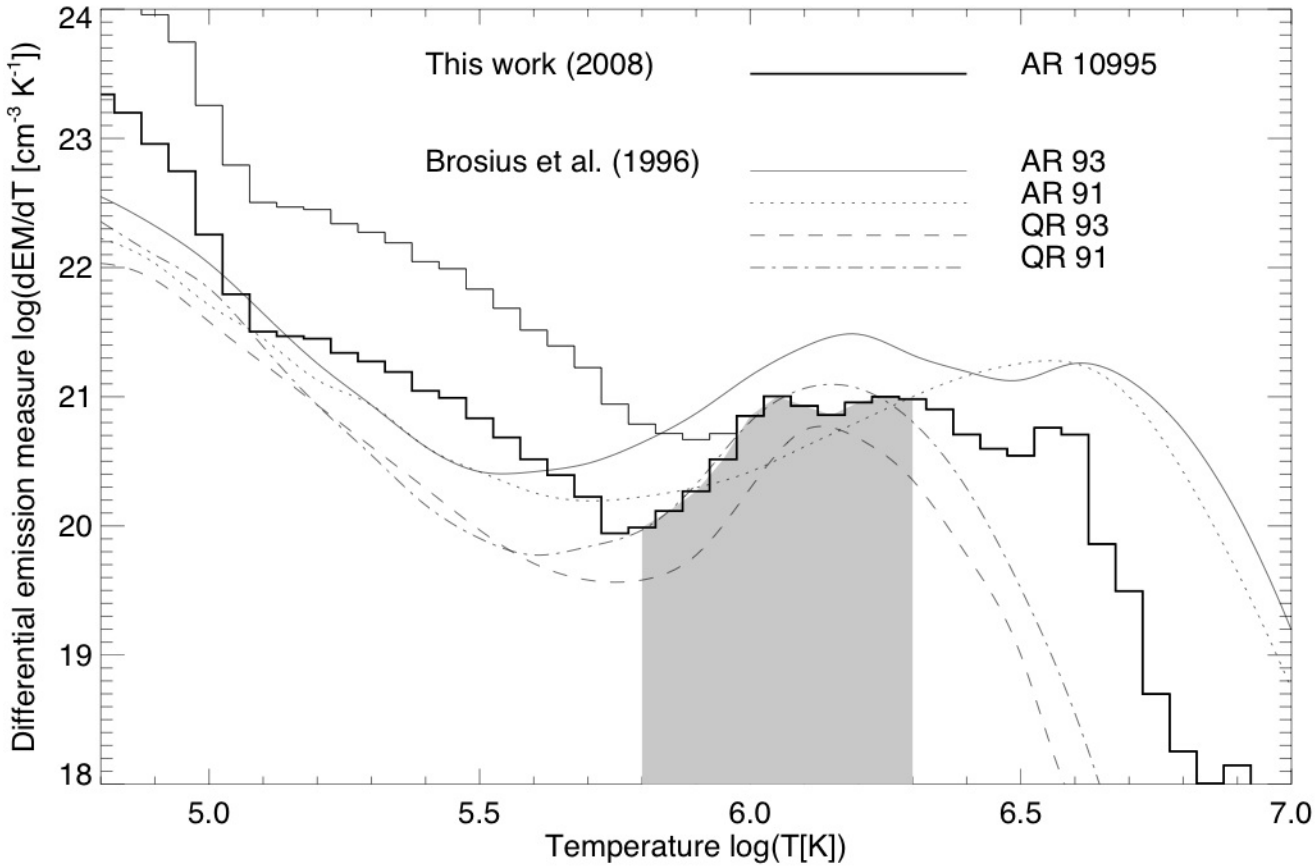

Differential emission measure distribution of forward-fitted AR model (with & without tapering of loop footpoints)

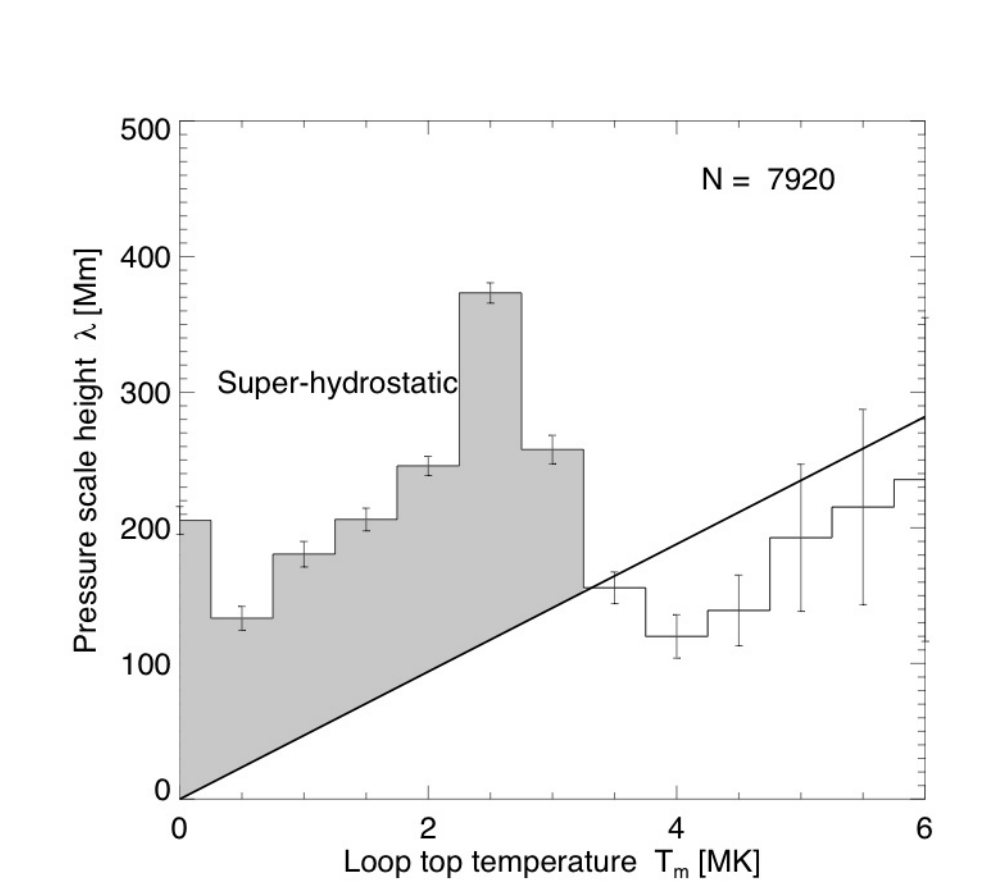

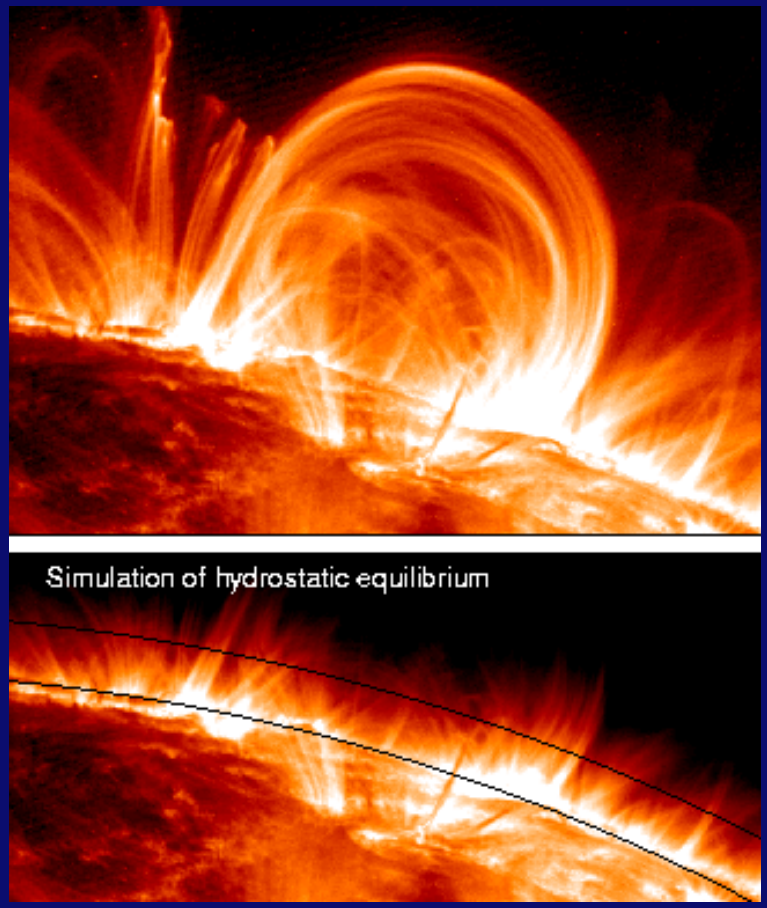

Forward-fitted AR model yields super-hydrostatic loops for T<3 MK

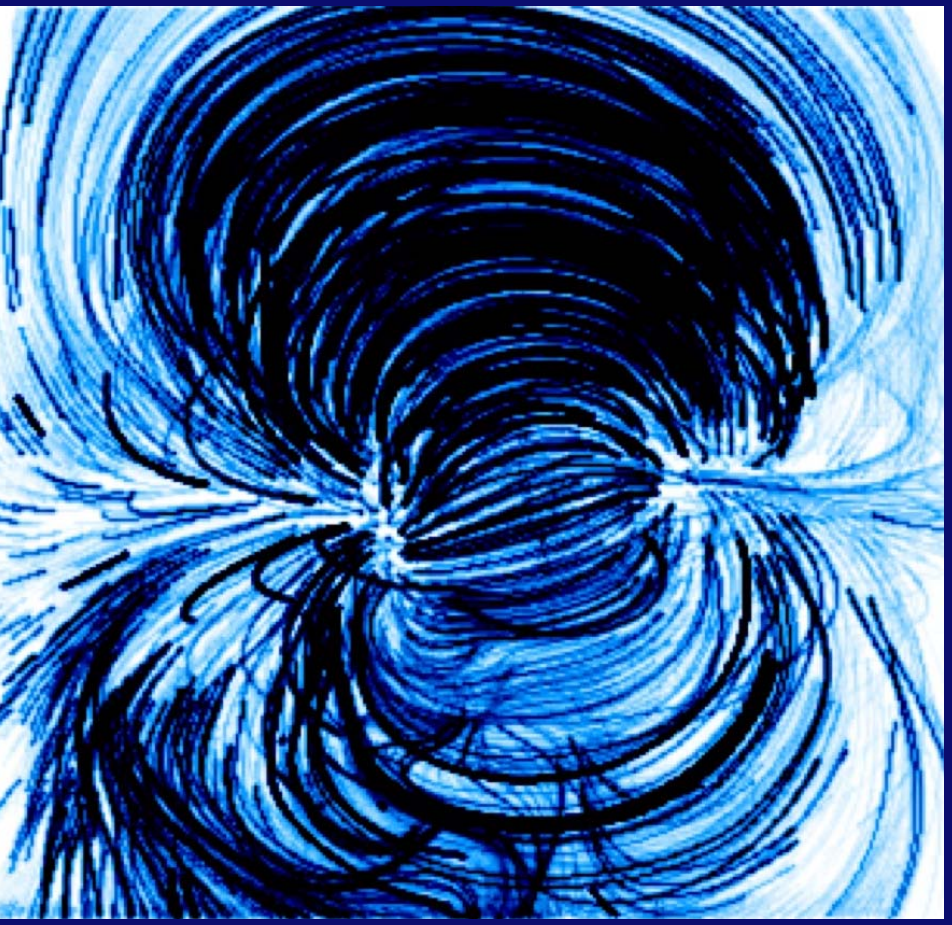

Density model

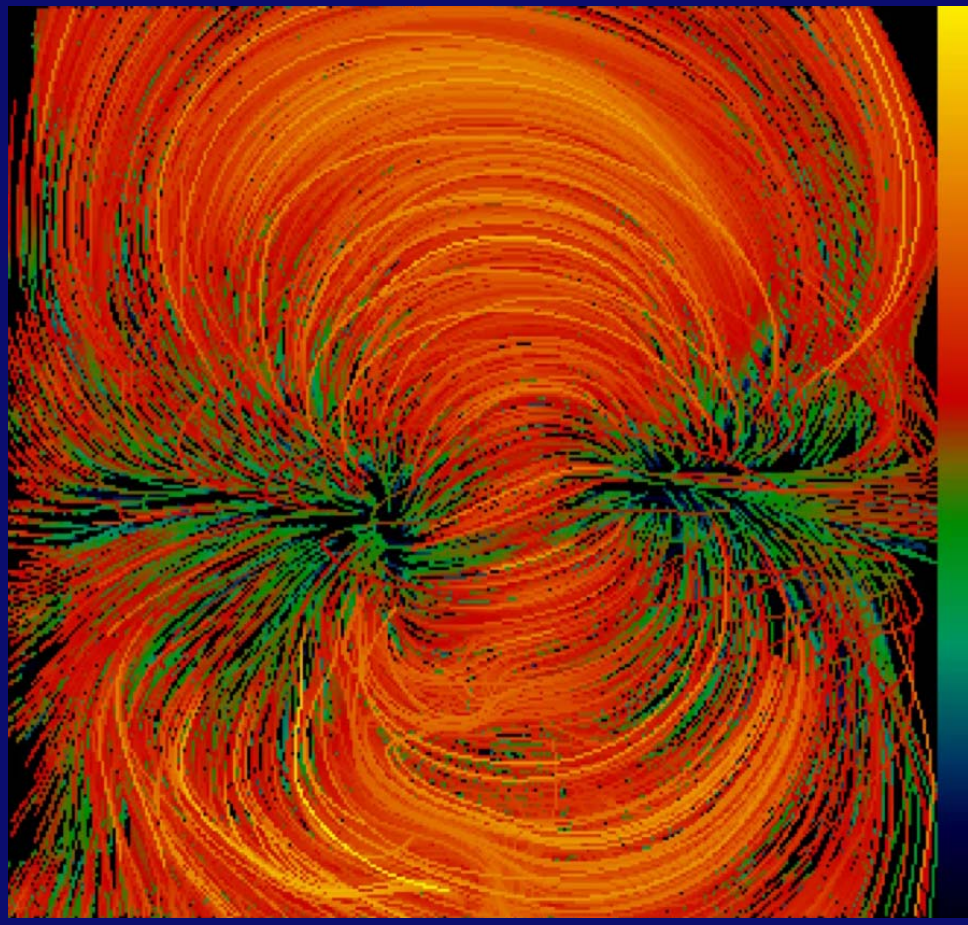

Temperature model

of forward-fit

Conclusions

(1) 2007 is the prime mission time for classical stereosocopy with small separation angles (<40^0). SDO will be launched when STEREO has very large separation not suitable for stereoscopy.

(2) The stereoscopic triangulation provides the 3D loop coordinates [x,y,z], the inclination angle of loop planes that is important for modeling the (hydrostatic) gravitational stratification, the LOS angle and projected loop widths for inferring the electron density.

(3) The dual stereoscopic view provides two independent background subtractions which yields a self-consistency test for the inferred physical loop parameters

(4) The 3D (x,y,z) coordinates of loops provide the the most accurate geometric constraints for magnetic modeling of active regions.

(5) Using stereoscopically triangulated loops as a skeleton, a 3D field can be interpolated and filled with plasma to produce a volumetric rendering of an active region, aiding forward-fitting in other wavelengths.